Aalto University
School of Engineering
Department of Mechanical Engineering

Janak Aryal

Characterization and optical imaging of dual-fuel combustion

Master's Thesis

Espoo, 14 November 2017

Supervisor: Prof. Martti Larmi

Thesis Advisor: D.Sc. (Tech) Ossi Kaario

Aalto University
School of Engineering

Aalto University, P.O. BOX 11000, 00076 AALTO
www.aalto.fi

Abstract of master's thesis

Author Janak Aryal

Title of thesis Characterization and optical imaging of dual-fuel combustion

Degree programme Degree Programme in Mechanical Engineering

Major/minor Personal minor **Code** K901-W

Thesis supervisor Prof. Martti Larmi

Thesis advisor(s) D.Sc. (Tech.) Ossi Kaario

Date 14.11.2017 **Number of pages** 66 **Language** English

Abstract

As the regulations for engine-out emissions around the world are getting increasingly stringent, dual-fuel (DF) combustion involving natural gas or methane as primary fuel ignited by a very small diesel pilot can be an attractive alternative to diesel only combustion in heavy duty engines of both road as well as marine applications. Natural gas or methane have potential for reduction of carbon dioxide emissions because of their high hydrogen to carbon ratio compared to diesel fuel. Their highly premixed combustion also produces less NOx than diesel as the overall combustion temperature is lower. Furthermore, they have huge potential for exploitation at competitive prices in regions such as India, China and North America, thus helping to reduce dependency on conventional diesel and gasoline.

In this thesis work, an attempt has been made to characterize the DF combustion of premixed methane and diesel pilot with the help of optical and thermodynamic measurements. DF combustion experiments were carried out in a single cylinder, optical research engine with electro hydraulic valve actuation system and custom made engine control program that enable research with great degree of parameter freedom. Crank angle resolved images of Natural Luminosity (NL) resulting from combustion were acquired using a high speed CMOS camera. NL signals showing the development of premixed flame fronts, cylinder pressure traces, heat release rate (HRR) profiles and ignition delays are considered as tools for characterizing the DF combustion in this thesis work. Influences of methane lambda (λ_{CH4}), of pilot fuel ratio (PR) and of charge air temperature on dual-fuel combustion were investigated separately using three different case studies.

From optical and thermodynamic investigations, it was observed that the ignition delay and shape of HRR in DF combustion strongly depend upon lambda of the gaseous fuel. With methane substitution rate ranging from 82% to 88%, when λ_{CH4} was varied from 1.1 to 1.9, it was observed that the periods of ignition delays were longer at both least as well as most lean case, with relatively shorter delays around the λ_{CH4} 1.5 region. The study of DF combustion as a function of PR revealed that the DF ignition delay decreased with increasing PR until a certain extent after which any increase in PR did not bring the ignition delay significantly forward. In the final case study, for both λ_{CH4} 1.1 and λ_{CH4} 1.8 cases, it was observed that higher intake temperatures shortened ignition delays, promoted second stage combustion and reduced cycle-to-cycle variations. However, at high intake temperatures, certain DF cycles also demonstrated excessive rates of pressure rise immediately after the onset of combustion. In summary, it is concluded that at high substitution rates (ca. 85%) and light load conditions as experimented in this thesis, DF combustion is dominated by the premixed flame front propagation mode rather than by the characteristics of diesel diffusion combustion.

Keywords dual-fuel, ignition, methane fuel, optical, flame front

Preface

This thesis was done at Internal Combustion Engine Laboratory, Aalto University. The thesis has been funded by the Academy of Finland (projects DF-Ignition and CleanGas) and European Union's Hercules 2 Project. I greatly appreciate the financial aid provided by these organizations and projects for the completion of this thesis. I am also grateful to Merenkulunsäätiö for a small grant the foundation provided me for completing this thesis work.

I would like to extend my sincere gratitude to Professor Martti Larmi and D.Sc. (Tech) Ossi Kaario for not only giving me an opportunity to work with this thesis in their projects but also for their role as thesis supervisor and thesis advisor respectively. Their guidance and feedback while completing this thesis work has been invaluable.

I would like to heartily thank Olli Ranta and Otto Blomstedt from the laboratory for their valuable technical guidance and help throughout this thesis work. Without their help, completing this thesis would not have been easy. I thank Zeeshan Ahmed, Tuukka Uosukainen, Rasmus Pettinen, Reetu Sallinen and Kari Hujanen for their advice and help at various stages of this thesis work and also for creating a collaborative environment in the laboratory.

I cannot thank enough my family for all the support and affection I have been getting throughout the completion of this thesis and otherwise in my life. This thesis is for you!

Espoo, November 14, 2017
Janak Aryal

Table of Contents

List of Abbreviations

AFR	Air to fuel ratio
ATDC	After top dead center
BTDC	Before top dead center
CAD	Crank angle degree
CI	Compression ignited
CMOS	Complementary metal-oxide semiconductor
DF	Dual-fuel
EHVA	Electro hydraulic valve actuation
FPGA	Field programmable gate array
HCCI	Homogenous charge compression ignition
HRR	Heat release rate
LHV	Lower heating value
NHRR	Net heat release rate
NL	Natural luminosity
PID	Proportional- Integral- Derivative
PR	Pilot fuel ratio
PREMIER	Premixed mixture ignition in the end gas region
PRR	Pressure rise rate
RCCI	Reactivity controlled compression ignition
SI	Spark ignited
SOI	Start of injection
SR	Substitution rate
TDC	Top dead center
TTL	Transistor- transistor logic

List of Symbols

c_p	Specific heat at constant pressure
c_v	Specific heat at constant volume
$\dot{E}$	Energy flow rate
h	Specific enthalpy
m	Mass
$\dot{m}$	Mass flow rate
p	Cylinder pressure
	Pressure
Q	Heat transfer
QHR	Cumulative heat release
Q_{gr}	Gross heat release
Q_{ht}	Heat transfer to walls
Q_n	Net heat release
R	Gas constant
T	Temperature
V	Cylinder Volume
	Volume
λ	Lambda
λ_{CH4}	Methane lambda
λ_{diesel}	Diesel lambda
λ_{DF}	Dual-fuel lambda
φ	Crank Angle
ϕ	Equivalence ratio
γ	Specific heat ratio

List of chemical compounds and emissions

CH_4	Methane
CO_2	Carbon dioxide
NO_x	Nitrogen oxides
SO_x	Sulphur oxides
OH*	Hydroxyl radical

1 Introduction

In recent decades, investments in research and quest for technological advancements in the field of internal combustion engines have been driven mainly by the need for emissions reduction. Legislations regulating the engine-out emissions are becoming increasingly stringent by the years. In order to meet these legislative demands of significantly reduced emissions, internal combustion engine manufacturers have turned to the development and use of sophisticated exhaust aftertreatment systems, cleaner combustion technologies and cleaner fuels. On the other hand, sources of the non-renewable fossil fuels around the world, especially of conventional diesel and gasoline, are fast depleting. As a result, vehicles, especially of heavy duty and marine type, and power generation industries of the world will have to look for developing and using alternative fuels as well as developing combustion technologies that can best utilize them. Interest in natural gas as a fuel for heavy duty and marine vehicles and for stationary power generation sets centers around these two issues.

In this thesis work, dual-fuel (DF) combustion involving methane as a primary fuel ignited by a small quantity of diesel called "pilot", is studied. Methane is the major component of natural gas, typically constituting more than 90% of it. In this thesis, industrial methane (99.8% pure) is used as gaseous fuel. Methane is considered a cleaner fuel compared to conventional diesel because of the theoretical reduction of CO_2 resulting from its higher hydrogen to carbon ratio. At lean mixture conditions, highly premixed combustion of methane reduces NOx as the combustion temperature is low. Combustion of methane also does not result in emission of SO_x, making it a cleaner alternative to heavy fuel oil in marine applications. Moreover, its vast potential for exploitation in regions such as China, India and North America means it can become a cheaper or at least economically competitive alternative to diesel and gasoline.

A dual-fuel engine, as the name suggests, uses two fuels, typically of different reactivity. In diesel-methane DF engine which is the subject of this thesis work, the combustion of methane which has lower reactivity, is initiated by the energy provided by compressed ignition of a pilot quantity of diesel fuel which has higher reactivity. Because of its high resistance to knock, methane can be used as primary fuel source in a conventional diesel engine with high compression ratio resulting in diesel like efficiency. This also means that minimum modification is required to the diesel engine to use it as a DF engine. Moreover, such a DF engine can be switched instantly to run purely on diesel fuel whenever it runs out of gaseous fuel or whenever it is economic to do so. In heavy duty and marine applications, DF engines such as *Wärtsilä 20DF, Wärtsilä 50DF* are already well known power generating devices. During light load operation and start up, such engines are generally run in diesel only mode and when the optimal operating temperature is reached, the diesel fuel is switched to pilot quantity with the rest of the fuel requirement being fulfilled by the gas [1].

In literature and industrial use, the term "dual-fuel" may refer to many different types of combustion that utilize two fuels, and thus needs some clarification. It is important to differentiate it from the "Gas Diesel" combustion where the gas is injected directly into the combustion chamber and burns as it is injected in the same manner as liquid diesel [1]. The ignition of the gas still has to be initiated by diesel pilot. In the context of this thesis work and also found mostly in literature, dual-fuel combustion refers to the technology where the combustion of a premixed charge of gaseous fuel-air mixture is initiated by the ignition energy provided by a pilot quantity of diesel fuel injected few crank angle degrees before the top dead

center (TDC). Owing to the difference in injection timing, gas equivalence ratio and stratification levels of the charge at the end of the compression stroke, it is also differentiated from the premixed charge compression ignition (PCCI) and reactivity controlled compression ignition (RCCI) combustion concepts. The DF combustion now distinguished from other combustion concepts utilizing two fuels, can still, in itself refer to different combustion regimes and operating strategies depending upon substitution ratio, equivalence ratio and fuel type [2].

A typical DF combustion process shares the characteristics of both premixed (or SI) and diesel (or CI) combustion processes. The process is therefore dependent both on the spray and ignition characteristics of diesel pilot as well as on the gaseous fuel type and its concentration in the mixture. The presence of gaseous fuel in the premixed charge brings variations in the physical and transport properties of the mixture as well as to the preignition processes of the diesel pilot [3]. Consequently, the ignition delay period gets prolonged in DF combustion mode compared to that in diesel only mode and the heat release rate profile also gets altered. Study of these variations provides tools for characterizing DF combustion at different operating conditions in this thesis work.

Two main issues associated with DF combustion that limit its operating window are knock and misfire. At high loads, if the gaseous fuel- air mixture is too rich, knock can occur. When autoignition of the end gas mixture ahead of the flame front propagation takes place in the vicinity of the pilot fuel sprays resulting in an uncontrollably rapid pressure rise, the phenomenon is referred to as knock. Consequent high temperature and increased heat transfer during knocking can quickly lead to engine damage [1, 3]. Conversely, at light loads if the mixture is too lean, a consistent flame front propagation of the premixed gaseous fuel-air mixture fails to develop, leading to misfire [4]. Under such circumstance, the unburned gaseous fuel escapes the cylinder, the phenomenon termed as ‘methane slip’, producing an increased emission of hydrocarbons. Thus, in order to ensure the operation of DF engine at maximum efficiency within a narrow window of equivalence ratio limited by the two issues of knock and misfire, the engine requires a sophisticated control system capable of controlling both air flow and pilot quantity.

Although as already mentioned, the use of DF engines is not any longer new in the industry, significant research is still needed to fully understand DF combustion in order to overcome the limitations that surround it. As pointed out by Dronniou et al [2], it is still not fully established whether the DF combustion is characterized by autoignition, flame propagation, diffusion or a combination of these modes. The following are therefore, outlined as the main objectives of this thesis work:

1. Produce optical evidences (i.e. combustion images) that can help reveal what combustion modes are dominant at different cases of equivalent ratio, intake air temperature and pilot fuel ratio
2. Accompany the combustion images with corresponding thermodynamic results such as ignition delays and heat release rate profiles and use them as tools for characterizing DF combustion
3. Make average as well as cycle-to-cycle study of DF combustion at varying combustion parameters

In each case study, crank angle (or time) resolved optical images of combustion development based on natural luminosity are obtained and these results are believed to contribute to the contemporary research in DF combustion that is focused on studying combustion stability, emissions, engine performance and efficiency. Optical study of DF combustion covering a parameter study as broad as being made in this thesis is very limitedly available in literature. In this thesis work, optical investigation is carried out in a free parameter, single cylinder, optical research engine with the help of a high speed CMOS camera.

2 Background

2.1 Combustion

In *internal* combustion engines, mechanical power is drawn from the chemical energy stored in fuel by oxidizing the fuel *inside* the engine. In four stroke engines, combustion of the fuel-air mixture that has been inducted into the engine is initiated towards the end of the compression stroke and near the top dead center (TDC) when the cylinder volume gets compressed to a small fraction of its initial volume. Combustion of the mixture is initiated either by an ignition source such as a spark plug as in the case of Spark Ignited (SI) engine, or by spontaneous ignition of portions of the mixture when the fuel's autoignition temperature is reached as in the case of Compression Ignited (CI) engine. During combustion, chemical energy stored in the fuel is released in the form of heat resulting in a rapid rise in cylinder pressure. The high temperature, high pressure gases in the cylinder push the piston down during the expansion or power stroke producing useful mechanical work. The form and manner of heat release is very much a function of the thermochemical reaction taking place between fuel and air during combustion, which in turn depends upon the characteristics of the fuel, the design of the engine's combustion chamber, fuel-injection system and the engine's operating conditions [5]. Hence, the combustion phenomena as such, are very different in SI and CI engines.

2.1.1 Premixed combustion

Premixed combustion requires that the fuel and air be mixed well before the ignition forming an ignitable mixture that is more or less homogenous and close to stoichiometric state ($0.8 \leq \lambda \geq 1.2$ in engines). In SI engines which employ premixed combustion process, fuel and air are mixed together either outside the combustion chamber by injecting fuel into the intake manifold or inside the combustion chamber as in Direct Injection (DI) systems by injecting fuel early at the beginning of the intake stroke, resulting in a fairly homogenous mixture. Portion of this mixture located near the ignition source (spark plug) is then ignited by a timed electric spark towards the end of compression stroke. Following ignition, a flame front develops and propagates through the premixed fuel-air mixture until it reaches the combustion chamber walls where it extinguishes [5]. In light of this, premixed combustion process is generally divided into four distinct phases: 1) ignition, 2) early flame development, 3) flame propagation, and 4) flame termination. The flame development and subsequent propagation is very much dependent on local mixture motion and composition [5]. Figure 1 shows flame front positions at different crank angle degrees (CAD) for two types of mixture formation systems on the left and for a four-valve engine with centrally located spark plug on the right.

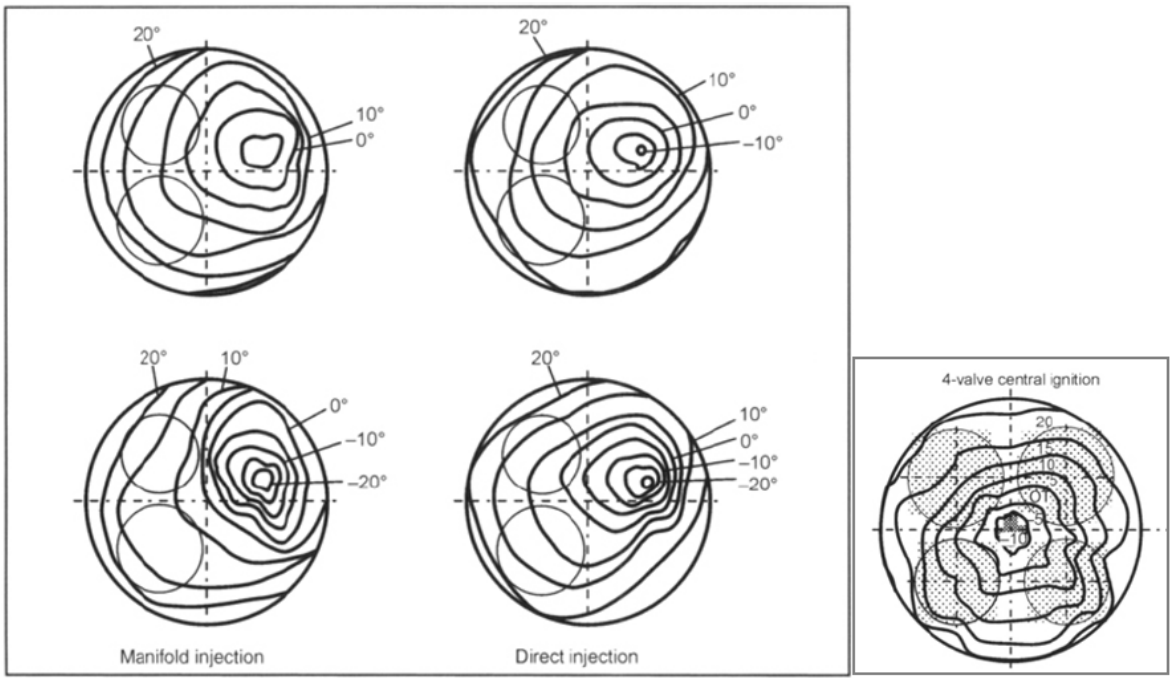

Figure 1. *Left: flame front propagation from two working cycles for injection into the intake manifold upline of the intake valve and for direct injection during intake stroke, λ = 1 mode; right: flame front propagation in four-valve engine with centrally located spark plug [6]*

According to van Basshuysen and Schäfer [6], an ideal case of a completely premixed flame is when flame propagation occurs in an absolutely homogenous fuel-air mixture in the combustion chamber. They further note that the chemical processes that take place at the flame front are slow compared to the heat and material transport processes and therefore, the premixed combustion is a chemically controlled process.

Heywood [5] defines a flame as the result of a self-sustaining chemical reaction occurring within a region of space called the flame front where unburned mixture is heated and converted into products. He also recognizes that the flame front consists of two regions- a preheat zone and a reaction zone. It is further noted that the preheat zone is where the temperature of the unburned mixture is raised mainly by heat conduction from reaction zone and where no significant reaction or energy release occurs. Then when a critical temperature is reached, exothermic chemical reaction releasing chemical energy as heat begins to take place. Reaction zone is the region between the temperature where this exothermic reaction begins and the hot boundary at the downstream equilibrium burned gas temperature [5].

Flame in premixed combustion process can have a laminar or a turbulent structure. A laminar flame is characterized by a laminar flame speed and a laminar flame thickness. Laminar flame speed is the velocity at which the flame propagates into quiescent premixed unburned mixture. And, one approach to defining the laminar flame thickness is to identify it as a ratio of the molecular diffusivity to the laminar flame speed. Laminar flame speed is dependent on the temperature and species concentration gradients within the flame [5].

However, in most combustion devices such as engines, it is desired to have premixed combustion process taking place in a turbulent flow field of the mixture. This is because turbulence leads to significantly greater increase in mass consumption rate of the reactants compared to that in laminar flames. Greater mass consumption rate means increased rate of

chemical energy release that is essential in engines [7]. Having conditions enabling turbulent flame front propagation is also important in engines from the point of view of spark timing. As the RPM of the engine increases, turbulence level increases meaning an increase in the mass consumption rate of the fuel-air mixture and thus, allowing for the use of an unaltered spark timing with respect to RPM changes in engine cycles [7]. In engines, turbulent flow field is generated by the high shear flows set up during the intake process (e.g. from intake channel shapes) and modified during compression [5]. While laminar flame speeds are typically in the range of 0.5-2 m/s , turbulent flame speeds can reach as high as 20-25 m/s depending upon charge motion (swirl, tumble, or squish). Thus, contrary to laminar flame speed, the turbulent flame speed is not only dependent on fuel-air mixture ratio, but also on the flow characteristics and configuration of the combustion volume.

2.1.2 Diesel combustion

As opposed to premixed combustion, time available for mixture formation is very short in diesel combustion. Fuel under high pressure (300-3000 bar) is injected either directly into the main combustion chamber (as in Direct Injection systems) or into the prechamber (as in Indirect Injection systems) towards the end of the compression stroke, typically few CADs before TDC. The injected fuel has to then atomize, evaporate, mix with compressed hot charge and then autoignite within a short span of time. Therefore, it is essential to have fast injection and best possible atomization of fuel that promote intensive mixture formation in diesel engines [6].

Spray formation or atomization, droplet evaporation, fuel-air mixing and combustion continue until essentially all the fuel has passed through each of these part processes which are highly interactive with each other. This makes the diesel combustion an extremely complex process that is highly dependent upon the characteristics of the fuel, on the design of the combustion chamber and fuel injection system and on the engine's operating conditions [5, 6].

Over the years, attempts employing chemical kinetics and laser based diagnostics have been made to understand the unsteady, heterogeneous and three-dimensional diesel combustion process [5]. One such attempt was made by John Dec [8] in his work titled " *A conceptual model of DI Diesel Combustion Based on Laser-Sheet Imaging"* in 1997 and his conceptual model depicting the evolution of DI diesel combustion from start of injection, SOI up through the early part of mixing-controlled burn has been widely used ever since. A schematic of that conceptual model in the form redeveloped by Flynn et al. [9] is presented in Figure 2 below. The figure which is very much self-descriptive shows regions of liquid fuel, fuel vapor- air mixture and diffusion flame in one diesel flame as it evolves from 1 CAD after SOI to 10 CAD after SOI when early mixing-controlled burn phase is reached.

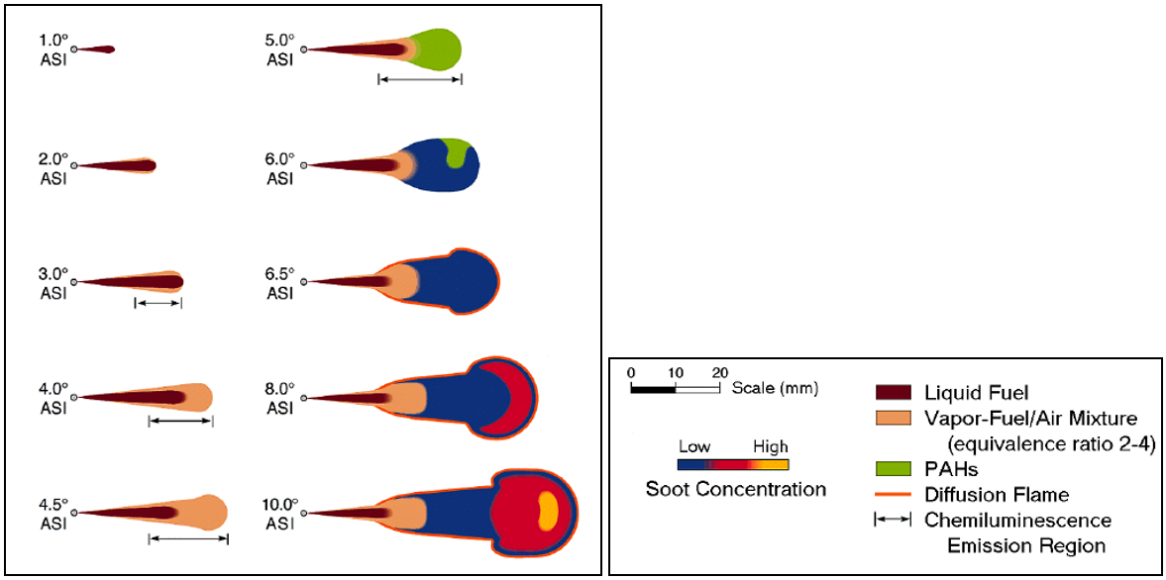

Figure 2. *Schematic representing conceptual model of diesel combustion [8, 9]*

Heat release rate is one of the methods of obtaining quantitative information about the progress of combustion (fuel mass burning rate being the other). It tells about the rate of release of fuel's chemical energy during the combustion process [5]. The mathematical expression for obtaining this heat release rate and assumptions made in the process are described later in Section 3.4.3. From a typical heat release rate curve as seen in Figure 3, four distinct stages of diesel combustion can be identified.

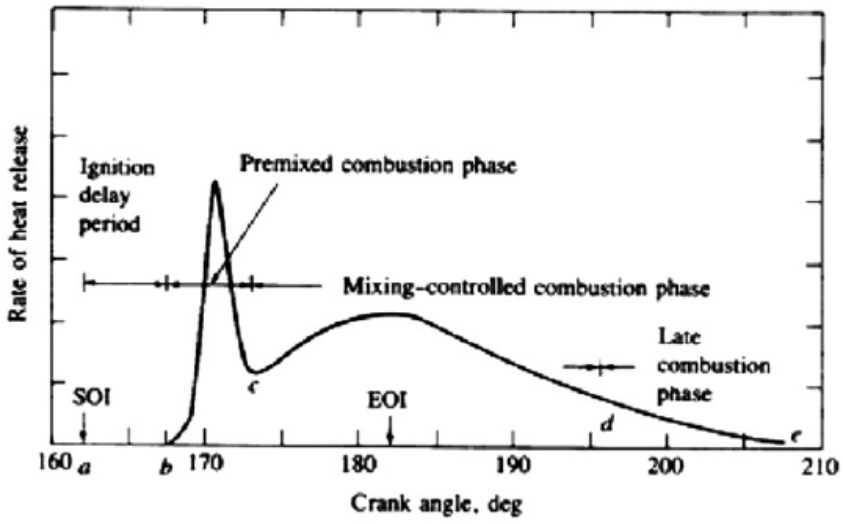

Figure 3. *Typical heat release rate profile at different phases of diesel combustion process [5]*

The four stages are:

Ignition delay: There's a period between the start of injection, SOI and the actual start of combustion which can be identified as a period of *ignition delay*. In Figure 3, it is the CAD interval spanning *a* to *b*. In this thesis work, ignition delay has been used as one of the prime factors for characterizing dual-fuel combustion and it is determined from the heat release analysis of cylinder pressure data and validated from the combustion images (time between SOI and first detection of any natural luminosity, NL signal).

Premixed combustion phase: According to Heywood, following the ignition delay, a phase spanning few CADs exists during which rapid combustion of the fuel that has mixed with air to within the flammability limits (more or less homogenous and reactive) during the period of ignition delay occurs. This phase, spanning *bc* in Figure 3 is characterized by high heat-release rate (HRR). Such HRR is credited to the fact that the mixture which has started burning in this phase adds to the fuel that has become ready for burning and actually starts burning late in the phase [5].

Mixing-controlled combustion phase: In the phase spanning *cd* in Figure 3, the rate of burning is primarily controlled by the fuel vapor and air mixing process. As several processes such as liquid fuel atomization, vaporization and fuel vapor-air mixture formation still continue strongly in this phase, it is characterized by *diffusion* combustion and is also referred to as the main combustion phase [5, 6].

Late combustion phase: The end of the combustion (span *de* in Figure 3) is marked by lower HRRs as the pressure and temperature in the diesel flame have dropped so much that the chemistry becomes slower than the mixing process taking place at the same time [6]. Heat release comes from some fraction of the fuel that might yet have not burnt or from fractions present in soot and other combustion products that get burnt during this phase [5]. This phase thus, becomes important from the point of view of exhaust gas emissions.

The form of the typical diesel combustion heat release rate curve discussed here gets significantly influenced and altered during dual-fuel combustion which involves small amount of diesel pilot and a large amount of premixed methane. In the later sections of this chapter as well as in the *Results* chapter, attempts have been made to detail this effect.

2.1.3 Dual-fuel (DF) combustion

In engines employing dual-fuel (DF) combustion concept, both SI like combustion and conventional diesel like combustion coexist together. The gaseous fuel and air mixture premixed in the intake port of a conventional diesel engine gets increasingly compressed in the cylinder as the piston approaches TDC. However, this mixture does not autoignite due to its high autoignition temperature. The ignition of this mixture is thus initiated by injection few CAD_S before TDC, of a small amount of diesel also termed as “pilot” fuel. The spontaneous ignition of diesel pilot which occurs when the in-cylinder temperature has reached its autoignition level, initiates nearly simultaneous ignition of premixed gas-air mixture at several locations depending upon the number of diesel injector holes (and thus, the number of sprays) [10, 11]. Following ignition and depending upon gaseous fuel concentration in the charge, a turbulent flame front propagation proceeds throughout the charge originating from pilot ignition regions. Thus, a typical DF combustion process is dependent both on the spray and ignition characteristics of the diesel pilot and on the property of the gaseous fuel and its overall concentration in the cylinder charge [3].

Reactivity Controlled Compression Ignition (RCCI) combustion concept also exploits the difference in reactivity of two fuels but differs from DF combustion because in RCCI concept, the high reactivity or high-cetane fuel is directly injected early in compression stroke to control the autoignition of premixed high-octane fuel. As such, the RCCI combustion is dependent only on the chemical kinetics of the combined fuels [12].

Four distinct stages of conventional diesel combustion were established in Section 2.1.2. However, in case of DF combustion, Sahoo et al. [10] have identified five stages based on cylinder pressure trace in their journal titled "*Effect of engine parameters and types of gaseous fuel on the performance of dual-fuel gas diesel engines- A critical review"*, published in 2008. The five stages of DF combustion identified by them and as seen in Figure 4 (right) are 1) pilot ignition delay (*AB*), 2) pilot premixed combustion (*BC*), 3) primary fuel ignition delay (*CD*), 4) rapid combustion of primary fuel (*DE*) and, 5) flame propagation stage (*EF*).

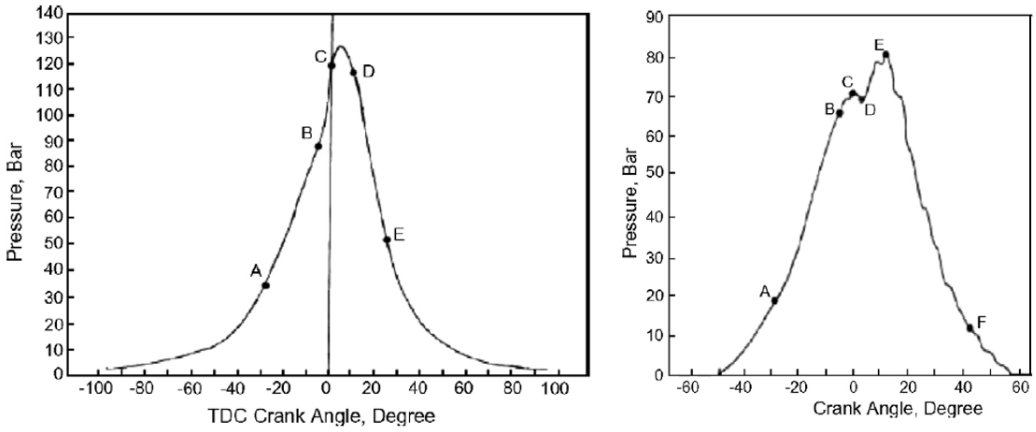

Figure 4. *In-cylinder pressure traces showing stages of diesel (left) and DF (right) combustion [10]. For diesel: AB = ignition delay, BC = premixed combustion, CD = mixing controlled combustion; DE = late combustion stage*

The pilot ignition delay (*AB*) is longer in DF combustion mode than in pure diesel operation mode, believed to be due to the reduction in oxygen concentration resulting from gaseous fuel substitution for air. The pressure rise *BC* following this delay is also lower than in pure diesel mode as only a small quantity of diesel pilot ignites in DF mode. Then, there's an ignition delay of the gas-air mixture and the pressure decreases slowly (*CD*) during this period until the actual combustion of this mixture commences. Flame propagation initiated by autoignition of diesel pilot results in rather unstable combustion phase that is marked by the pressure rise *DE*. At the end of this rapid pressure rise, flame propagation still continues well into the expansion stroke (*EF)*.

The HRR profile in DF combustion process is a result of contribution from three overlapping components according to Karim [3]. Schematic representations of these components in DF heavy load condition and low load condition are presented below in Figure 5.

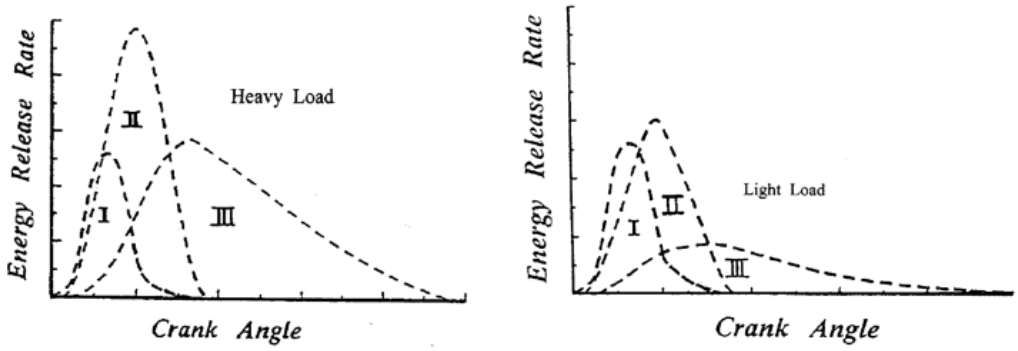

Figure 5. *Schematic representation of different components of HRR in DF combustion at heavy (left) and light load (right) conditions [3]*

The first component, *I* of HRR results from the combustion of the diesel pilot, the second, *II* is contributed by the combustion of gaseous fuel portion lying in the immediate vicinity of pilot ignition regions and the third, *III* is due to gaseous fuel-air mixture preignition reactivity and subsequent flame front propagation. The second and third components of HRR are relatively smaller in contribution in light load case as a consistent flame propagation struggles to take place in this case where the gaseous fuel-air mixture is very lean [3]. While the extent of contribution from components *I* and *II* is a function of the diesel pilot quantity, that from the third component, *III* is associated with the concentration of the gaseous fuel. Azimov [4] et al. have identified a possible fourth component that contributes to the HRR in DF combustion. It is argued that in lean burn conditions, this additional contribution to HRR comes from the autoignition of the mixture in end-gas region (but not knocking) that happens simultaneously with flame front propagation; and the phenomenon has been called PREMIER (PREmixed Mixture Ignition in the End Gas Region) combustion [13].

PREMIER combustion

The PREMIER combustion mode has a narrow operating range that lies prior to the onset of knocking combustion (Figure 6). However, a marked improvement in thermal efficiency and reduction in smoke emission provide motivation for developing strategies that can lead to the extension of this operating window.

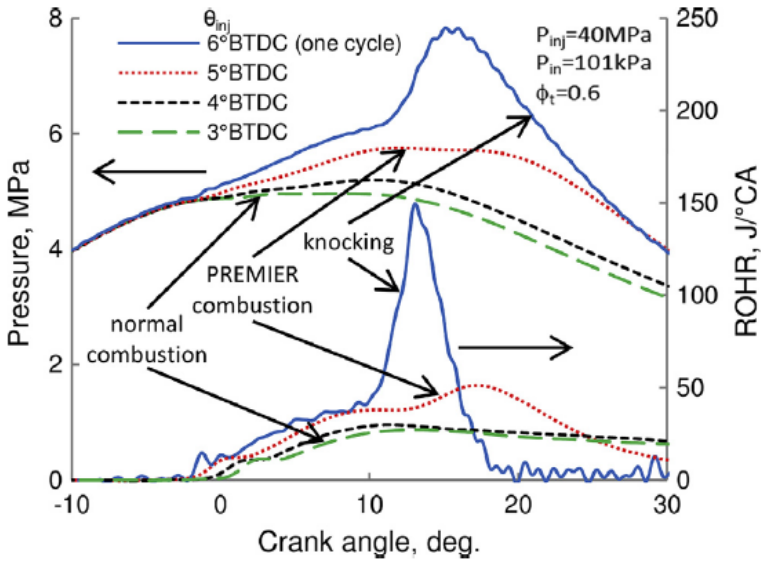

Figure 6. *Typical pressure traces and HRRs of normal, PREMIER and knocking combustion [13]*

While in the normal combustion process a flame front moves completely across the combustion chamber in a uniform manner and at a normal velocity, in knocking combustion, portions or all of the charge may autoignite in the end-gas region at extremely high rates. If however, the DF combustion is controlled in such a manner that the mixture does not autoignite spontaneously during or following the rapid release of pilot energy, but instead well away from the initial ignition regions, a PREMIER combustion mode can be established. This needs a precise parametric combination of mainly diesel pilot injection timing and EGR rate (as it affects equivalence ratio based on oxygen content) and to a lesser degree of pilot quantity and injection pressure. Under lean gaseous fuel-air mixture conditions, as the flame front propagates, some mixture remains unburned, located beyond the boundary of the flame front

and at the same time the temperature and pressure of the end-gas rises because of the end-gas compression. As a result, the unburned mixtures gets preheated throughout the combustion chamber volume, and when the end-gas reaches autoignition point, simultaneous autoignition occurs in several limited locations, known as exothermic centers, with a sharp, yet controlled rise in heat release. The resulting PREMIER combustion mode is different from knocking combustion with regards to the size, gradients and spatial distribution of the exothermic centers [4].

Ignition delay in DF combustion

Ignition delay in DF combustion mode shows markedly different trend compared to pure diesel combustion mode as observed by Karim [3]. As can be seen in Figure 7, for DF combustion that uses any gaseous fuel, the delay first increases with the increase in total or duel-fuel equivalence ratio and then, after a certain maximum point, it tends to decrease to a minimum before reaching the total stoichiometric ratio.

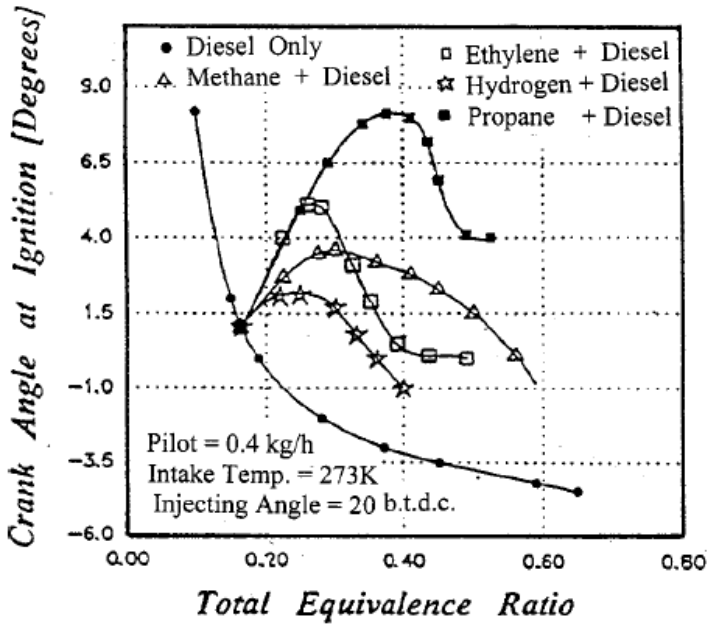

Figure 7. *Variations in start of ignition time with total (DF) equivalence ratio for different fuels at constant diesel pilot [3]*

The admission of gaseous fuel in DF combustion affects the ignition delay for a number of reasons. As the gaseous fuel is injected into the intake port to mix with intake air, the physical and transport properties of the mixture get affected. In addition, the pre-ignition reactivity of diesel pilot gets affected when the intake partial pressure of oxygen changes with the air displacement by gaseous fuel. Furthermore, it has been shown that the gaseous fuel type and its concentration in the charge influences significantly the heat losses during compression and thus, the peak temperature at TDC resulting into variations in ignition delay [3].

2.2 Influence of parameters on DF combustion and DF engines

DF combustion behavior and consequently the DF engine operating window are affected by a number of parameters such as pilot fuel ratio, equivalence ratio, intake air temperature and pilot injection parameters and strategy. Understanding of the influence of these parameters available from literature is presented in sections below.

2.2.1 Influence of lambda

Lambda, λ is defined as the ratio of the actual air-to-fuel ratio to the stoichiometric air-to-fuel ratio. In preceding sections of this document, its reciprocal, the fuel-to-air equivalence ratio (ϕ) has been mentioned with regards to different aspects of combustion. Both terms will be continued to be mentioned in this document, but λ will be recognized as the parameter to be studied.

In the context of DF combustion involving diesel and methane, three different lambdas need to be identified- diesel lambda, λ_{diesel}; methane lambda, $\lambda_{CH4;}$ and the total or dual-fuel lambda, λ_{DF}. While the diesel and methane lambdas are related to air-to-fuel ratios associated with respective fuels only, the total or dual-fuel lambda is related to air-to-combined fuel mass ratio (formulation is found in section 3.4.1). The influence of λ_{diesel} on diesel pilot ignition or DF combustion is not so significant as diesel combustion is more dependent on spray behavior and mixture formation. With small percent of diesel pilot quantities (or pilot fuel ratio, PR in the context of this work) used, λ_{DF} is less than but near to λ_{CH4}. Thus, the influence of λ_{CH4} on DF combustion is quite significant as it not only affects the flame front propagation of the methane-air mixture but also the time of the onset of diesel ignition (ignition delay).

The effect of λ_{DF} on ignition delay has already been discussed in the end of section 2.1.3. The same trend is associated with λ_{CH4}, as most of the combined fuel mass is contributed by methane. When it comes to flame propagation, under high λ_{CH4} conditions, premixed flame front is too weak to propagate and thus may extinguish resulting in incomplete combustion and emission of fractions of methane, also referred to as methane slip [3, 4]. On the other side of the spectrum, under low λ_{CH4} conditions when the mixture is too rich in gaseous fuel, knock will occur due to the autoignition of the premixed gaseous fuel-air mixture in the vicinity of diesel pilot sprays [1]. As such, the operating range of a DF engine is quite narrow, bounded by the lean and rich limits of methane. Figure 8 shows optimal operating window with respect to λ_{DF} and load axes for Wärtsilä DF engines that use only a few percent of diesel pilot [14]. λ_{CH4} in itself however, is not an independent parameter of influence in DF combustion, as the misfire and knock limits are greatly affected also by the gas properties, charge air temperature and compression ratio.

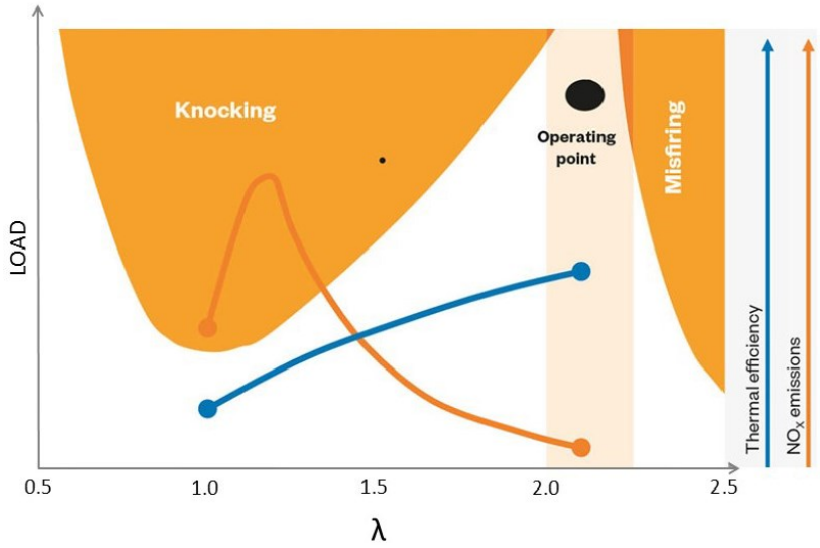

Figure 8. *Operating window for Wärtsilä DF engines [14]*

2.2.2 Influence of pilot fuel ratio

Pilot fuel ratio (PR) is the share of the total injected energy provided by diesel pilot. The diesel pilot ratio influences whether the DF combustion leans more towards CI or SI combustion behavior. It also strongly influences the controllability, performance and emissions of DF engine. With low pilot fuel ratio, DF combustion is dominated by premixed combustion behavior and thus is more reliant on the gaseous fuel concentration in the charge. Under such condition, the second component of HRR and its overlap with the third component outlined in section 2.1.3 are small resulting in an overall lower HRR trend and combustion temperatures [3, 12]. At part load operation, very small diesel pilot quantity coupled with low charge air temperature may even lead to ignition failure. At increasing diesel pilot ratios, flame area of premixed gaseous fuel-air mixture in DF combustion becomes increasingly dominated by diesel combustion. Abd Alla et al. [15] argue that larger pilot provides a large pilot fuel envelope and a greater multitude of ignition centers with larger reaction zones resulting in bigger volume of premixed charge that become engulfed in the vicinity of the pilot combustion zone. This also means that there's a greater overlap between the second and third components of HRR and the combination of these two produces increased HRR immediately after the pilot autoignition [3]. While at low loads, increasing the share of diesel pilot leads to successful flame propagation, at high loads, increasing it beyond certain limit might lead to early knocking [15].

Since diesel and methane have different stoichiometric air-to-fuel ratios, AFR (14.5:1 for diesel and 17:1 for methane), a change in diesel pilot ratio also produces a change in the total or DF stoichiometric AFR and thus, requires corresponding air mass flow adjustments during engine operation.

2.2.3 Influence of charge air temperature

The effective mean temperature of the fuel-air mixture inside the cylinder during the period of ignition delay greatly influences the preignition physical and chemical processes [16]. Among many factors affecting this effective main temperature near TDC, the intake or charge air temperature is also an important one (refer to formulation in Section 3.4.2 which shows

relationship between initial charge temperature and TDC temperature). It has been observed by Karim and Burn [17] that at very low intake temperatures and especially with small pilot quantities, ignition delay increases significantly leading to a tendency to erratic engine running or even ignition failure. In this thesis work, with pilot quantity kept very small (0.35 kg/h), it is attempted to observe the influence of raising the intake temperature from ambient conditions at two different extremes of gaseous fuel admission, one that gives λ_{CH4} 1.8 and another that gives λ_{CH4} 1.1. Increase in intake temperature is expected not only to affect the ignition delay but also on the rate of pressure rise and heat release.

2.2.4 Influence of diesel pilot injection timing and pressure

Diesel injection parameters such as injection pressure and timing play influential roles in dual-fuel operation. Injection pressure directly affects diesel pilot spray atomization, penetration and vaporization which translates to an effect on mixing of pilot fuel with the premixed charge as well as on the distribution of ignition sites. At high injection pressure, higher amount of diesel fuel leaves the injector earlier, the fuel spray atomizes better, entrains and mixes with premixed charge faster and penetrates longer into the combustion chamber. Khosravi et al. [18] observed in optical investigation of diesel and natural gas DF combustion that under such conditions of high injection pressure, the autoignition of partially-premixed diesel mixture took place at the periphery of combustion chamber and the reaction zone then propagated towards the center in the form of a turbulent flame propagation of the gaseous fuel-air mixture. On the contrary, at low injection pressures, the diesel pilot spray cannot penetrate as long and mixing is limited. Under such conditions, they observed that ignition zones were localized around the vicinity of diesel pilot jet and a more heterogeneous autoignition of the gaseous fuel-air mixture was prevalent. This difference in distribution of ignition zones depending upon diesel injection pressure is also important from the emissions formation point of view.

Diesel pilot injection timing or SOI has direct influence on start of combustion and energy release in relation to the piston position, on peak cylinder pressure and ultimately on the efficiency of the dual-fuel engine. At a given λ_{DF} or λ_{CH4}, advancing the SOI results in increased peak cylinder pressure because much of the fuel burns near or before TDC where the temperature and pressure resulting from volumetric compression are the highest. If SOI is retarded, temperature and pressure during autoignition of diesel pilot is less than that would be at TDC which delays its ignition, and the temperature of the mixture at that point might not be enough to propagate the flame through the whole gaseous fuel-air mixture resulting in incomplete combustion. Although, a detailed case study of different SOIs will not be presented in this thesis, the described phenomenon was very much evidenced during the early stage parameter verification of thesis work, and therefore, the SOI was optimized by numerous trials so that the pilot fuel ignition initiated close to TDC.

2.3 Limiting factors in dual-fuel combustion

Since a DF engine shares the characteristics of both CI and SI engines, it also comes with both the advantages and disadvantages associated with these combustion types. The main advantage is that one can draw efficiency in DF engines that is higher than in both diesel and SI engines. There are two reasons for this. Firstly, the DF engine is basically built upon a conventional diesel engine which uses higher compression ratio than an SI engine. This already translates to an increased efficiency for DF engine compared to a normal SI engine. Secondly, combustion occurs quickly in a premixed charge present in DF engine than during diffusion burning in diesel combustion [19]. This means that the DF engine can operate in near ideal Otto cycles resulting in higher efficiency compared to diesel cycle at the same compression ratio. However, depending upon operating and gaseous fuel-air mixture conditions, the DF engine can be limited by both spark and diesel knock as well as by misfires.

2.3.1 Spark and diesel knock

Spark knock that is commonly associated with SI engines can be observed in DF engine also. This occurs due to the autoignition of the end gas, usually in the neighborhood of the diesel pilot spray. The temperature and pressure of the end gas rises because of its compression as the flame front propagates away from ignition zones and when its autoignition temperature is reached, the end gas burns very rapidly ahead of the flame resulting in rapid energy release and severe pressure rise rate that is detrimental to the engine. In DF engines, spark knock is attributed to too rich gas-air mixture, high intake temperatures and higher ratios of gaseous fuel substitution [1, 19].

When the pressure rise rate just after the start of diesel combustion is too high, the phenomenon is known as *diesel knock*. If the diesel fuel is injected so early before TDC that the conditions in the cylinder have not yet reached sufficient levels to cause its autoignition, it instead has enough time for forming a premixed mixture. When this premixed mixture eventually burns, severely rapid rate of pressure rise results that may be beyond the tolerable limits of engine design. In DF engine, the presence of premixed gaseous fuel-air mixture increases the ignition delay of diesel pilot compared to what it would be in normal diesel mode, and this can lay the ground for major fraction of diesel pilot to form a premixed mixture which when autoignites can lead to unacceptable rates of pressure rise. A pressure rise rate that exceeds 10 bar/CAD is generally considered unacceptable [20].

2.3.2 Misfire

Already in Section 2.2.1, the influence of λ (especially of λ_{CH4} as high substitution ratios are involved) on DF combustion has been discussed. When λ_{CH4} is too high (usually more than 2.1), the gaseous fuel-air mixture is too lean on methane and a consistent flame front propagation struggles to exist under such conditions. The premixed mixture might burn only partially or if it is too lean, might not burn at all resulting in *misfire*. This can lead to increased cyclic variations and unstable engine running as well as increased emissions of unburned hydrocarbons. In DF engine operation, the risk of misfire at light loads when the mixture is lean can be mitigated by increasing the ratio of the diesel pilot in total injected fuel.

Since the optimum operable window between the limiting factors of knock and misfire is quite narrow for a DF engine, it needs a sophisticated engine management system capable of controlling air flow and diesel pilot quantity amongst several other control parameters.

2.4 Optical investigation of dual-fuel combustion

2.4.1 Optical investigations of combustion in literature

Qualitative as well as quantitative information about the nature and progress of different types of combustion in engines can be drawn from optical investigative methods that usually employ a combination of optical access into the combustion chamber, high speed photography and some form of laser based techniques. In recent years, common technique to get optical access to a part of the combustion chamber in engines has been the use of either a Bowditch type piston with borosilicate, quartz or sapphire glass window installed on its top (example in Figure 17), or similar glass window holes placed on side walls of the cylinder near the head. Glass window holes on side walls of cylinder can also be used to transmit laser sheet through in investigative methods that use laser based techniques. Earlier optical investigative methods have often used endoscope based measurement systems. Some versions of engines with optical access can be run in conditions quite close to that of normal engine operation while most others have slight to heavy modifications to combustion chamber design and have short run times owing to the mechanical limitations and fouling of glass window in use.

Figure 9 shows optical result depicting the progress of diesel combustion (SOI: 9 CAD BTDC), obtained by Larsson [21] in his work *"Optical Studies in a DI Diesel Engine"* in 1999. He used an endoscope to get optical access of one of the four sprays coming out from a diesel injector, a light guide connected to a flash unit to illuminate the diesel spray prior to combustion and a color CCD camera connected to the output of the endoscope. Using some image post processing routine, namely the color separation method, he was able to show the diesel liquid fuel spray, its penetration into the combustion chamber, flame lift-off and flame length. Moreover, as can be seen in the figure, in the same work, he also used two-color method to extract information on temperature and soot distribution in diesel flame. Mathematical equations utilizing color intensity values present in image data, transmissivity of optical materials used and spectral radiance values amongst others are applied in commercial software to obtain such information. Details of such calculation methods are omitted in this document as they are beyond the scope of this thesis work. Larsson's result shows that optical measurement techniques can be used to draw both qualitative as well as quantitative information about combustion in engines.

Studies employing various other optical measurement methods intended to understand different aspects of combustion such as liquid fuel spray behavior, premixed flame propagation, knock, species concentration and distribution, dual-fuel and RCCI combustion etc. are available in literature. In 1997, Dec [8] used laser sheet imaging to model the evolution of a reacting diesel fuel jet from SOI to the end of injection which incorporates information on liquid and vapor fuel zones, fuel-air mixing, autoignition, reaction zones and soot distribution. A schematic of this outcome has already been presented in Figure 2 in Section 2.1.2. Similarly Arnold et al. [22] were able to get qualitative information about diesel fuel spray penetration using laser shadowgraphy and were also able to distinguish vapor and liquid phase in fuel distribution using laser induced fluorescence (LIF) and Mie scattering images. By taking LIF image pairs at different CADs of formaldehyde (CHOH*), a cool-flame intermediate species formed during the first stage ignition of hydrocarbon combustion, Bladh et al [23] visualized flame propagation in an SI engine with glass top piston and quartz ring in upper part of cylinder liner.

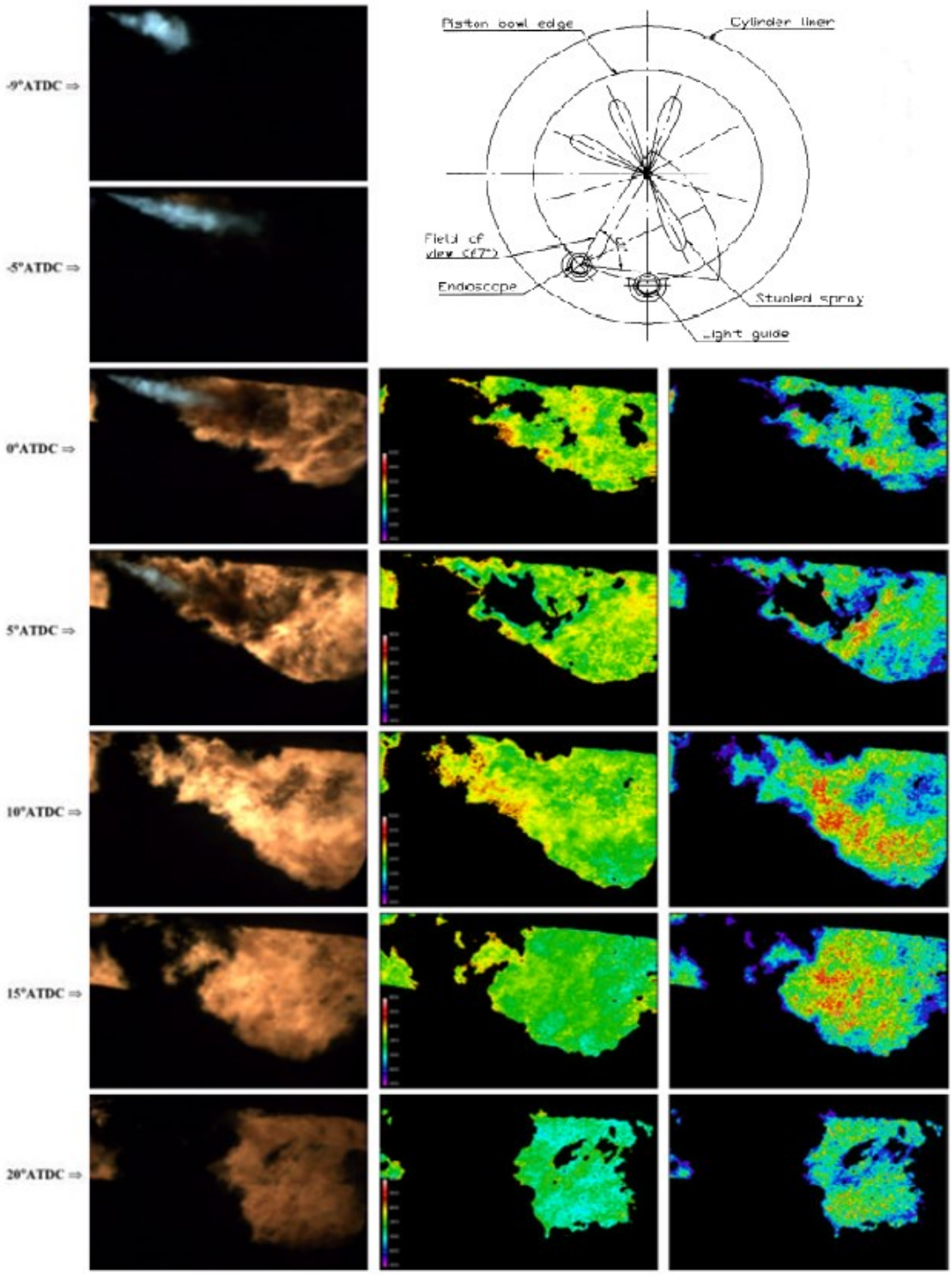

Figure 9. *Images set obtained by Larsson in [21] showing the progress of diesel combustion of one spray with respect to CAD. Small flame region on the left located below the nozzle does not belong to the spray in study. In the left column, liquid fuel spray and subsequent diesel flame can be seen. In the center column, temperature distribution (purple to red corresponding to a range of 1800 to 3000 K) is seen. In the right column, soot distribution in the flame (purple: thin soot, red: dense soot) is given.*

When it comes to optical investigation of DF combustion, it is worth mentioning the work done by Dronniou et al. [2] in their experiment with diesel-CNG DF combustion performed over a wide range of premixed fuel equivalence ratios. They made crank angle resolved imaging of combustion natural luminosity (NL) and one per cycle imaging of OH* chemiluminescence simultaneously. Furthermore, they accompanied these measurements with 2D Planar Laser Induced Fluorescence (PLIF) imaging performed in motored condition in order to characterize the mixture distribution of diesel pilot and distribution of premixed CNG fuel at ignition timing. They used six hole nozzle diesel injector and injected a pilot of 1.2 mg/cycle. It was observed in their optical results that at premixed equivalence ratios as low as 0.56, although the combustion starts near the walls of the piston bowl and then extends rapidly towards the center, the very central region within the bowl is devoid of NL signal indicating that the flame propagation is weak at such conditions. On the other hand, at premixed fuel richer conditions ($\varphi > 0.8$), it was observed that the flame originating from piston bowl walls progressively engulfed the fresh charge in the center wholly, indicating more complete combustion. The OH* chemiluminescence signal which is an indicator of high temperature oxidation reaction was consistent with NL signals in their result. The reason for flame propagation initiating from piston walls in DF combustion as opposed to from the center of combustion chamber as found in conventional SI engine has been attributed to the presence of higher local equivalence ratio near piston walls at the time of ignition observed in their PLIF images. Although this observation is open for discussion, a similar trend was observed by Kokjohn et al. [24] in a larger bore engine and also by Nithyanandan et al. [25] in their recent investigation in a light duty optical engine. Other notable visualizations of varying DF combustion strategies can be found in work done by Aksu et al [13] where they explore the possibility of extending PREMIER combustion operation range using split pilot injection and in that by Schlatter et al. [26] where they attempt to explain the root of increase in ignition delay of pilot spray (n-heptane) with increasing methane content using schlieren images that show density gradients of the premixed mixture. In the latter case, experiment was conducted in a rapid compression expansion machine.

2.4.2 Investigation of DF combustion based on natural luminosity

Sometimes, optical investigation involving only high speed imaging of natural luminosity resulting from combustion suffices to reveal many details about the evolution of combustion. Many optical studies of DF combustion available in literature are based on capturing NL images; sometimes they are complemented with OH* chemiluminescence imaging. In diesel-methane DF combustion, the intensity value of blue premixed flame is much lower than that of the sooty diesel flame, so a careful choice of camera exposure and post processing in the form of image enhancement are required to get intensity information from both flames. Overexposure to sooty and intense diesel flame can risk saturation and damage of camera CCD or CMOS chip.

Figure 10 shows NL images depicting the evolution of DF combustion involving diesel pilot (2 mg/cycle) and natural gas on the left (A) and diesel pilot and syngas on the right (B) [27]. In the images it can be seen that, after a finite period of ignition delay, premixed flame fronts initiate from the pilot fuel ignition regions and then propagate to consume the entire fuel-air mixture. Bright glow of soot particles in diesel flame is present throughout the combustion. The ignition delay in diesel-syngas DF combustion is considerably longer than in diesel-natural gas DF combustion, owing to the presence of CO_2 and CO in syngas.

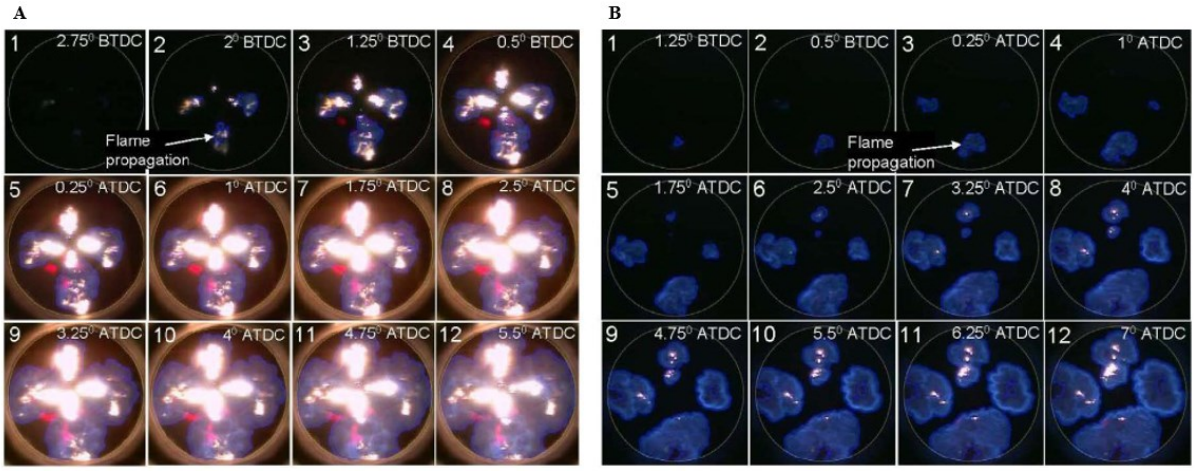

Figure 10. *Crank angle resolved NL mages of DF combustion: A) of diesel- natural gas, B) of diesel- syngas [27]. Diesel injected at 8 CAD BTDC.*

Together with cylinder pressure traces and HRR curves, NL images obtained in this thesis work are expected to reveal similar details about the progress of DF combustion- the ignition delay, ignition zones, early premixed flame development and subsequent propagation.

3 Methods

Configurations of the two engines (all-metal and optical) used for tests, parameter setup for experiments, protocols of tests and methods of measuring and analyzing cylinder pressure and optical images are discussed in the sections of this Chapter.

3.1 All- metal engine setup

Experiments for dual-fuel optical imaging in this thesis work were primarily carried out in a single cylinder research engine with optical access, the details of which will be discussed in Section 3.2. However, in the early stages of the experimental work, an all-metal counterpart of this optical engine was used as a test tool for trying different operation strategies and protocols that lead up to the parameter setup that can be experimented in the optical engine. Since the borosilicate glass window of the optical engine has thermal and pressure load limitations, the operating points of interest such as pilot fuel injection quantity, primary fuel quantity and charge air variables were first tested in the all-metal engine to monitor resulting combustion (read cylinder pressure) and forecast potential pitfalls of glass window failure in the optical engine.

The other goals of making early test runs in all-metal engine were to monitor certain metrics such as fuel mass flow rates that are not possible to measure during short runs in the optical engine and to test the performance of the diesel injector which had certain numbers of its nozzle holes clogged by welding. Since, the optical engine is just a counterpart of the metal engine with the added modification to its piston and cylinder that provide optical access, it shares much of its configuration with the all-metal engine.

3.1.1 Configuration

The all-metal engine is based on AGCO 84AWI 6-cylinder, common rail diesel, modified for single-cylinder research in dual-fuel application. The 6-cylinder diesel engine with total displacement volume 8.42 L is used in off-road applications. The geometrical dimensions of the engine in single cylinder modification are kept intact from the original 6-cylinder version. Important dimensions, measures and specifications of this single cylinder engine are listed in Table 1.

Table 1. All- metal test engine specifications

Cylinder bore (mm)	111
Stroke (mm)	145
Total Displacement- 6-cylinder (L)	8.42
Displacement 1-cylinder (L)	1.4
Compression ratio	16.5:1
Diesel pilot injection	Bosch CRIN3-20 Common rail, direct
Methane injection	Port injection with 2 Hana injectors
Engine control	Custom made in LabVIEW environment, uses NI DRIVVEN and other NI modules

This all-metal engine is a very flexible research engine which provides possibilities to freely vary all kinds of physical variables that could otherwise be restricted in normal engine

operations. The free control of parameters related to intake, injection, valve actuation, exhaust etc. is made possible by LabVIEW based and custom made control program that uses Field Programmable Gate Array (FPGA) provided by National Instruments.

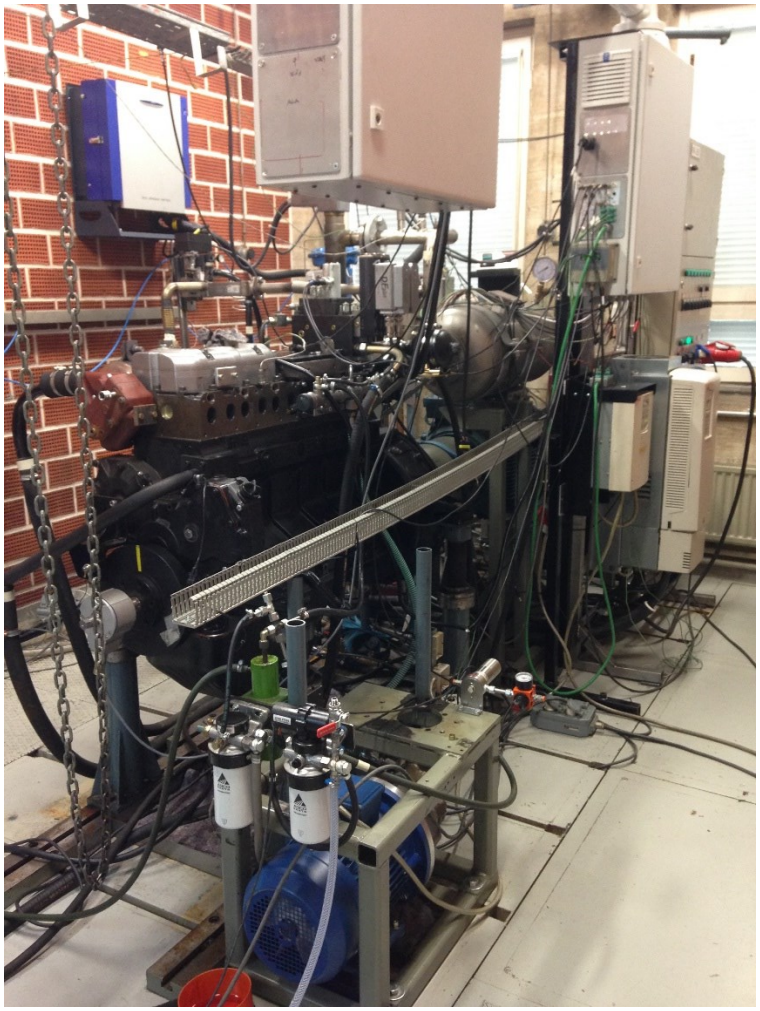

Figure 11. *All-metal engine setup*

An Electrohydraulic Valve Actuator, EHVA system provides for a camshaft-less gas exchange system in this all-metal (as well as optical- Section 3.2) engine setup. The intake and exhaust valves of the engine are actuated by high pressure hydraulic fluid and therefore, provide a possibility to control the valve lifts to follow various kinds of profiles without a need to change any hardware or physical component of the engine.

The configuration of this all-metal engine with its charge air, diesel and methane feed systems is schematically depicted in Figure 12. In single cylinder modified configuration, the engine is not always capable of producing the required work to maintain the requested engine speed. This depends upon quantity of injected fuel, resulting combustion profile and requested speed. In order to overcome this limitation, an AC-motor based unit in combination with a speed controlling frequency converter is connected to the engine crankshaft. The action of this combination is to drive the engine at requested speed when the engine itself does not produce enough work (or even when there's no combustion) and to brake the engine to requested speed when the engine produces work greater than the losses. This setup allows the user to rotate the engine at desired speed and stabilize air mass flow before injecting any fuel and thus, makes it possible to start the combustion with the right injection parameters. Moreover, the engine

does not stop with any possible misfire or braking thus allowing for parameter combination studies at such points.

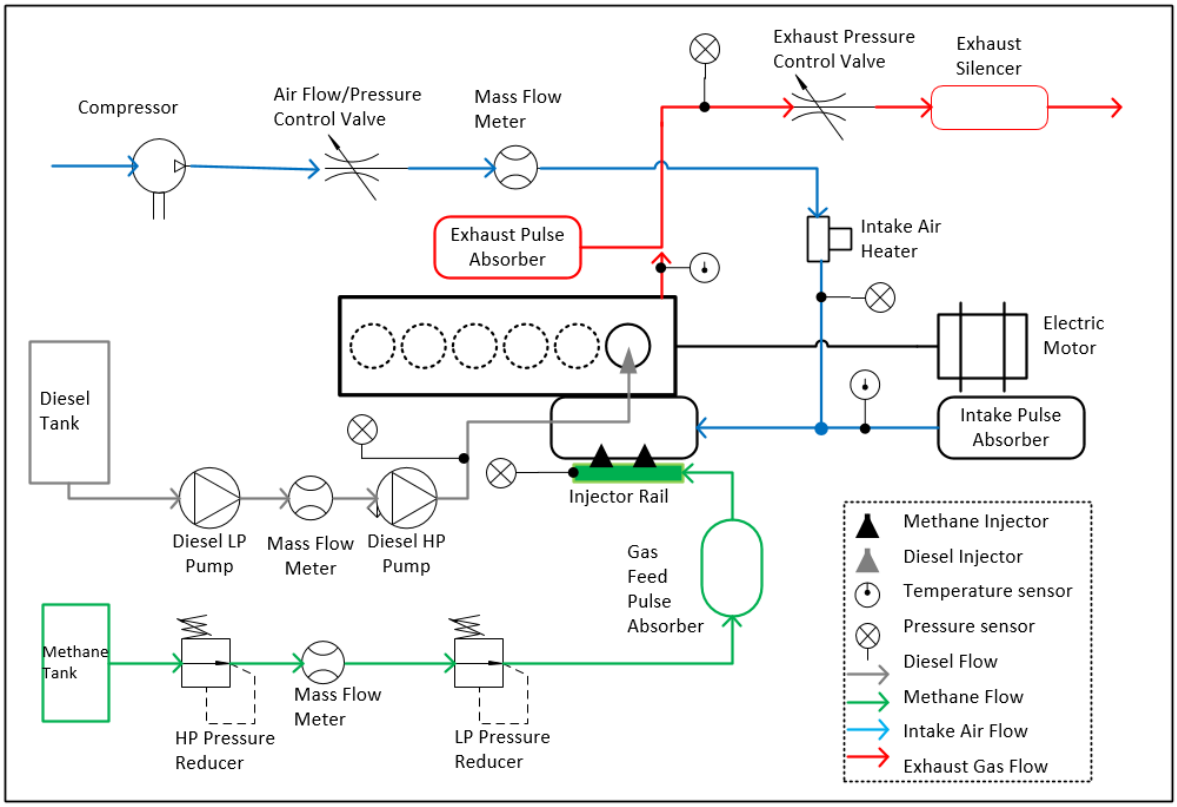

Figure 12. *Schematic of LEO I configuration*

3.1.2 Charge air feed system

The all-metal engine (or the optical) is not equipped with any turbocharger, but instead the charge air entering the cylinder can be boosted by an external industrial type air compressor. The maximum pressure that can be gained by this compressor is 8 bars, although such high boost is never necessary in this work. An external heating core also exists in the charge air feeding pipe, the temperature of which can be controlled by the user. The temperature of the charge air after the heater is always measured approximately half a meter before the intake manifold. The charge air mass flow into the cylinder is controlled with the help of an electronic butterfly valve placed after the compressor and before the air heater. The opening of this valve during engine run can be controlled by manual position request or by a PID controller in relation to requested boost or air mass flow rate.

As seen in Figure 12, the exhaust system of the engine consists of a simple piping with a pulse absorber and an exhaust pressure control valve with which the user can set some back pressure to replicate the operation of a turbocharged system.

3.1.3 Diesel injection system

Diesel injection system for the engine consists of a diesel fuel tank, two low pressure pumps for transferring diesel fuel from tank to a filter and then to a high pressure pump, a (common) rail and an injector (Figure 12). The rail pressure as well as diesel injection parameters can be controlled in real time during engine runs using the user interface of the LabVIEW based

engine control program. The required pressure (minimum at 800 bar to maximum at 2000 bar) is generated in the rail with an AC motorized high pressure pump equipped with a frequency converter and a PID controller. The injector is driven by an NI DRIVVEN module called DI (Diesel Injection) driver which provides a possibility to control the injector with its specified peak and hold currents and durations.

The injector used in this work is a Bosch CRIN3-20 common rail type intended for commercial vehicles in Tier4final applications (agriculture, forestry etc.). Originally, injector has 9 nozzle holes, each of diameter 0.138 mm. The minimum duration corresponding to combined peak and hold currents that can be used with the injector is 350 µs. Since this minimum feasible duration is still not small enough for flowing very small amounts of diesel pilot quantity used in this work, 7 out of 9 nozzle holes were blocked by welding.

Possible problems of modifying injector in this fashion are leakage from welded holes and injector tip overheating. Since very small nozzle holes were welded manually, there always existed some risk of them leaking. The extent of leakage in this work however, can be established during optical measurements. Diesel fuel flowing through the injector acts as a coolant of the injector tip. Recommended injector tip temperature during normal continuous operation is 300 ^{o}C and when the diesel fuel flowing through the nozzles is very small as in this work, the tip could be overheated resulting in hole size and clearance changes or complete failure by melting. The risk of injector tip overheating is mitigated at least in the optical engine by the fact that diesel injection and therefore combustion is initiated only once in every seven cycles.

A Coriolis type flowmeter placed in the diesel fuel line between the fuel transfer pumps and high pressure pump allows for measuring the fuel mass flow rate during engine runs.

3.1.4 Methane feed system

As seen in configuration schematic in Figure 12, the methane feed system consists of methane tank, high pressure regulator, Coriolis mass flow meter, low pressure regulator, gas feed pulse absorber, methane rail and two injectors. At the start of the feed system is a 50 L methane bottle containing 99.8% industrial methane at 200 bar when full. Immediately, after the bottle is attached a pressure regulator which reduces the pressure of the gas coming out of the bottle and into the feed pipe to 20 bar. A Coriolis type flow meter placed into the feed pipe after this regulator and before the Keihin pressure regulator is used to monitor the gas mass flow during engine runs. The function of Keihin pressure regulator is to further reduce the 20 bar pressure in the feed pipe to a pressure of 2.4 bar relative to the intake manifold pressure as the gas approaches the rail and the injectors. From the rail, two Hana manufactured gas injectors (Figure 14) inject methane fuel into the intake manifold. The injectors which have minimum opening time of 2.2 ms and closing time of 1.2 ms are driven by NI DRIVVEN module intended for Port Fuel Injection (PFI). It is worth noting that a gas feed pulse absorber (see schematic in Figure 12), which is basically a cylindrical vessel of approximately 15 L in volume, is placed in the feed system before the rail in order to compensate for methane mass flow losses during pressure fluctuations in the rail at the time of injection.

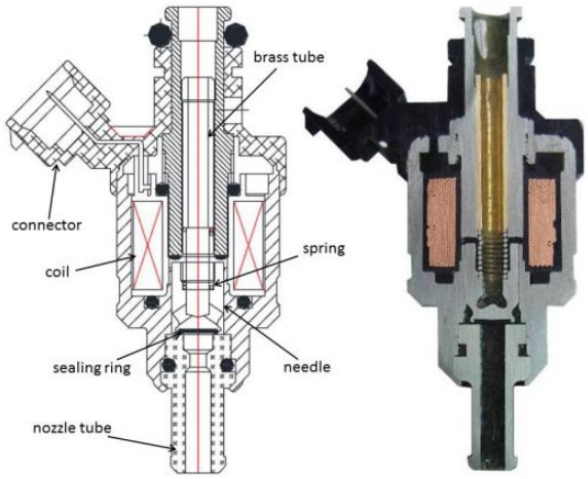

Figure 13. *A cross-section of a methane injector*

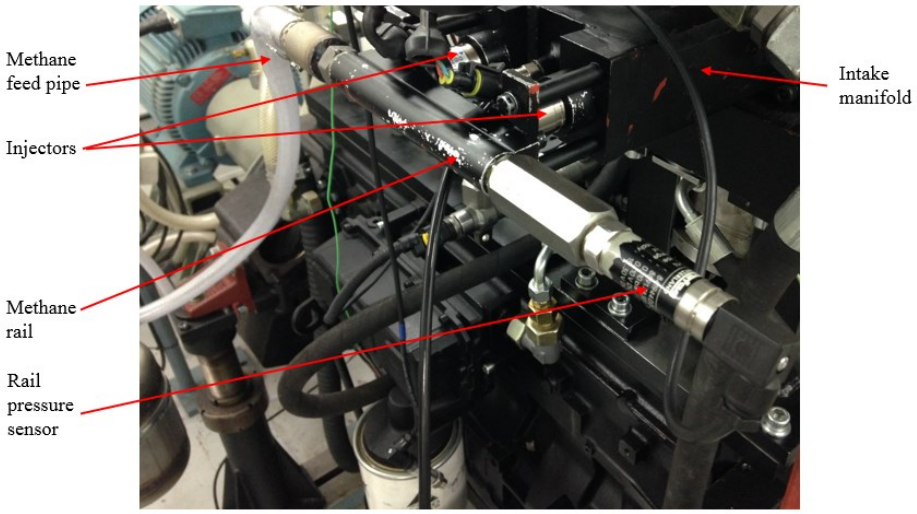

Figure 14. *Methane rail and injectors*

3.2 Optical engine setup

The optical engine, named LEO II (Low Emission Optical II) and used in this work has much of its configuration as well as engine control program, valve actuation, charge air feed, diesel fuel injection and methane feed systems similar to that of the all-metal engine as explained in Sections 3.1.1 to 3.1.4. Thus, unless specified differently hereafter, description of different setups made in those sections apply for the optical engine also. As such, only those aspects of the engine which differ from the all-metal engine setup and that provide optical measurement possibilities will be highlighted in this section.

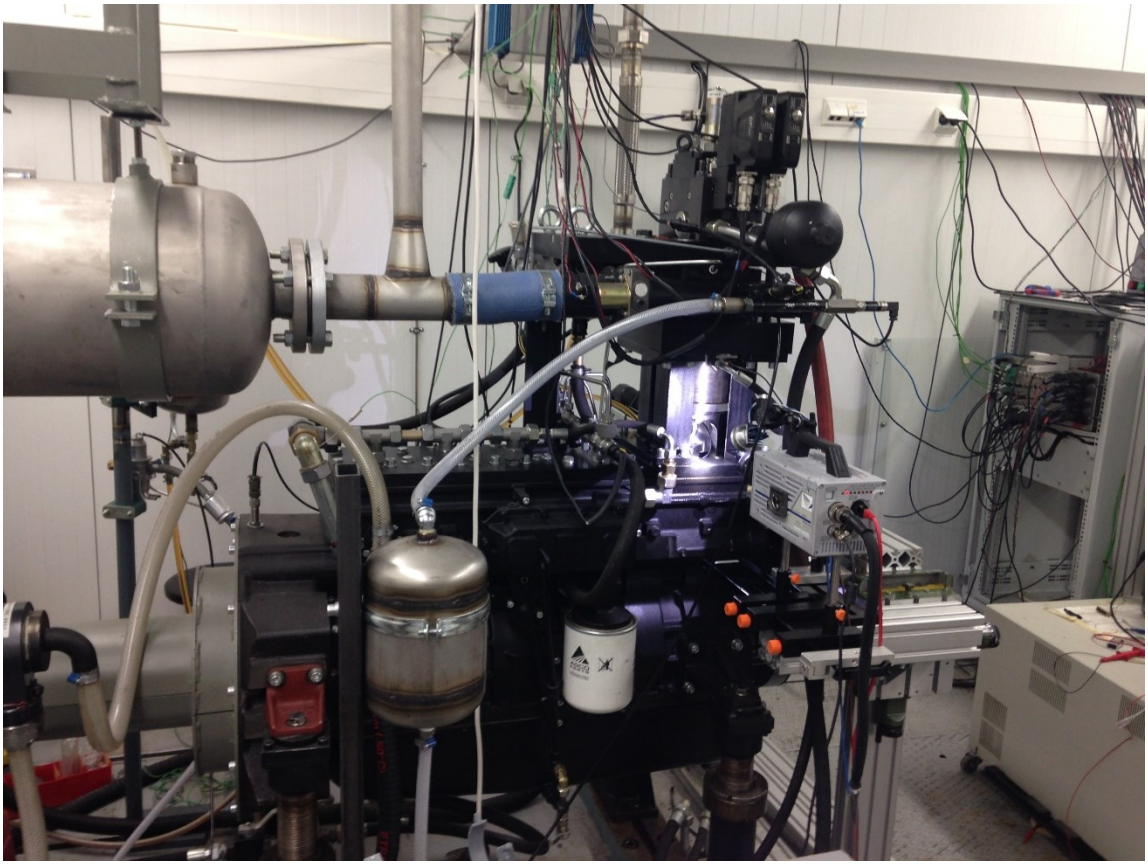

Figure 15. *Optical engine (LEO II) setup with high speed camera installed in place*

The key difference in the single cylinder optical engine to that of the all-metal engine is the modification of the original piston into a Bowditch piston in order to provide optical access of the combustion chamber. This means that the cylinder head of LEO II gets raised from the normal position by the scale of the piston extension (Figure 15). Also, the crown of the Bowditch piston is a flat dish with smaller depth compared to the deeper bowl head of the all-metal piston (Figure 16) and this results in a higher compression ratio (17.9:1) for the optical engine as the combustion volume at TDC becomes relatively smaller.

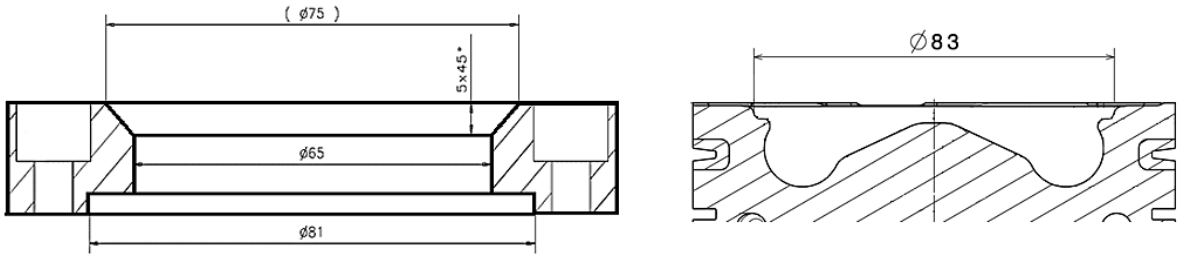

Figure 16. *Piston crown shapes of optical piston (left) and all-metal piston (right)*

The diesel line in optical engine setup does not have a Coriolis flow meter installed because the flows in this engine are very small owing to the combination of two factors- very small pilot quantities and use of skipfire protocol, and as such, available flow meter is not capable of measuring accurately such small flows. However, absence of flowmeter does not lead to any uncertainty in optical measurements as only those injection parameters that are validated with flow measurement in all-metal engine runs during early-stage parameter verification are used.

In the optical engine, where it is desired to limit the maximum cylinder pressure below the failure limit of the optical window, the EHVA system proved to be useful in tweaking the total mass flow of charge into the engine by freely reducing the maximum intake valve lift until a small enough mass flow was reached. Small charge air mass flow rates enable to use small injected energies (and thus smaller pressure levels) and still maintain the desired range of AFR.

3.2.1 Optical access

Optical access of the combustion chamber in LEO II is made possible by a Bowditch piston with borosilicate window as seen in Figure 17. The Bowditch piston has an extension made up of Titanium that is on lower end attached with the help of screws to the top of the original metal piston (aluminum) and at the other end, with the help of thread to an optical piston (also of aluminum). The borosilicate glass window that provides optical access to the combustion chamber is housed in this optical piston, sandwiched between its two segments bolted together. While the bottom (original) piston part uses original cast iron rings, the top optical piston part uses rings made of polytetrafluoroethylene (Teflon). The glass window provides an unblocked view equal to a diameter of 65 mm into the combustion chamber. The Bowditch piston reciprocates within a cylinder liner that has a cooling jacket and that is held in place with the help of two fastening bolts screwed to the cylinder head.

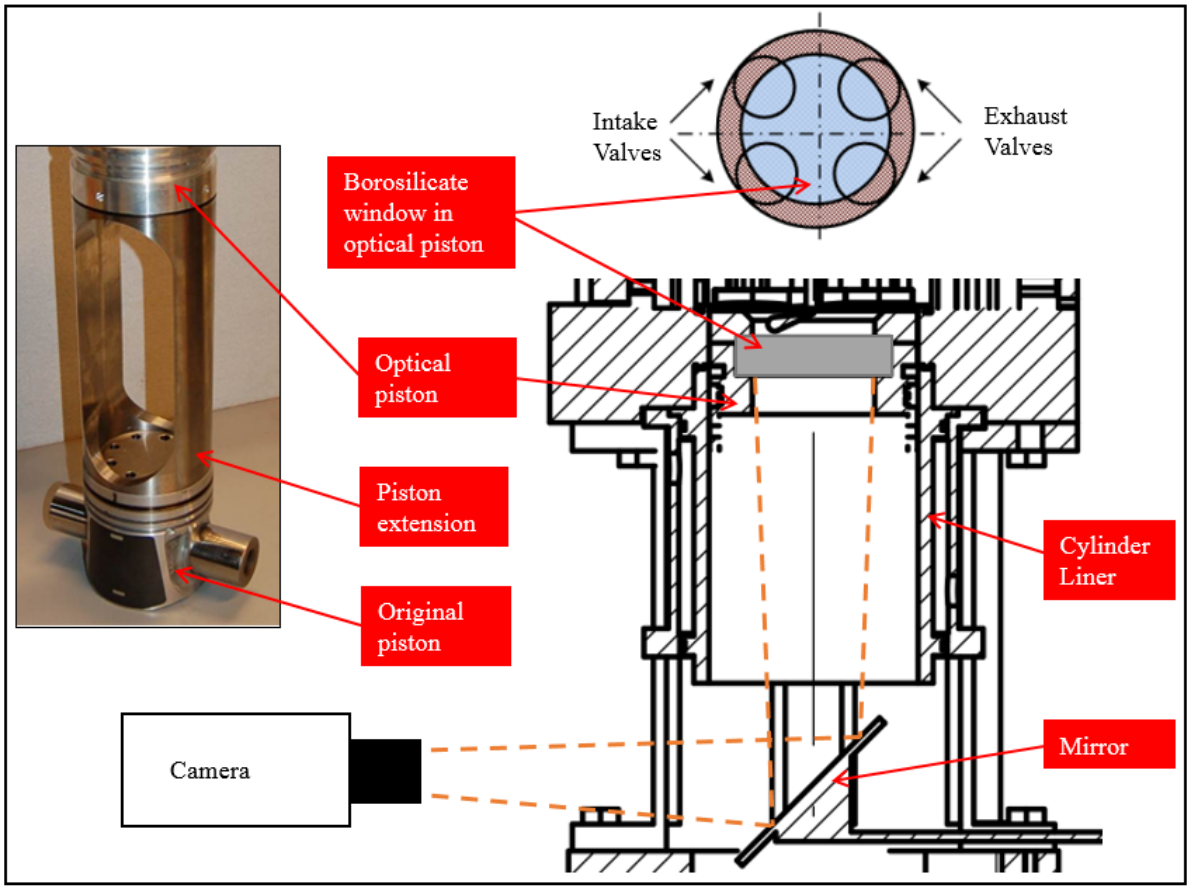

Figure 17. *Schematic representation of optical access through piston in the optical engine*

The glass window held in the optical piston gets dirty quite easily after a few combustion cycles. The dirt results from soot deposits from diesel combustion as well as from some drops of lubricating oil that find their way into the chamber. Therefore, the glass window is cleaned after every 100-150 injections. The cleaning is made rather easily- when the piston is rotated to bottom dead center, the cylinder liner can be pulled down to rest on the engine block by unfastening the two locking bolts and the glass window can be wiped clean with hand.

As already mentioned, the thermal and pressure loads that the optical piston can withstand is relatively less than the all-metal piston. In order to ensure that the window does not break because of the thermal loads, a skipfire protocol is used in tests. With the skipfire protocol, diesel pilot is injected into the cylinder once every seventh cycle. With regard to the pressure load, it had been established previously with tests in the research facility that the borosilicate window can withstand pressures up to 90-100 bars. So the peak cylinder pressures during tests were kept under this limit by using small enough total injected energies and charge air flows (based on early stage parameter verification in all-metal engine).

3.2.2 Natural luminosity imaging system

Combustion inside the cylinder is captured utilizing Natural Luminosity (NL) by a high speed CMOS camera installed in front of the mirror placed at 45° to the piston window (Figures 15, 17, 18). The camera used is Photron FASTCAM SA3 model capable of taking grayscale images at up to 120,000 fps with 128x16 pixels image resolution. However in the optical measurements performed in this work, it was desired to use 6000 fps record rate resulting in 512x512 pixels images covering the whole visible extent of combustion chamber. At 1400

RPM engine speed used in this work, this record rate meant that images are obtained at 1.4 CAD resolution. The camera is triggered externally from the LabVIEW based engine control program with respect to every pilot fuel injection signal and some 75-100 images are collected per trigger. These numbers of images cover well the span of combustion in each cycle. Further details and specifications about the imaging system can be found in Table 2 below.

Table 2. Optical measurement (imaging) system description

Camera	Photron FASTCAM SA3 model 120K- M3, monochrome
Type	High speed CMOS
Lens	Nikon AF NIKKOR 70 mm- f/4.5
Frame rate	6000 fps
Aperture	f/11
Exposure time	10 µs
Image resolution	512x512 pixels
Triggering	External, TTL signal from engine control program

Figure 18. *Photron FASTCAM SA3 camera*

The borosilicate window (10 mm in thickness) of the piston has transmission close to 95% for light above 400 nm in wavelength, so the visible light spectrum above this wavelength is captured well by the camera in the absence of any filters.

3.3 Experimental methods

3.3.1 Early stage parameter verification

In this thesis work, three different case studies regarding DF combustion were made. At this point, the reader is made clear that the all-metal engine in this thesis work was used only for early-stage parameter verifications that may or may not be directly related to individual case studies and therefore, all detailed case studies are actually performed in the optical engine. The three case studies were separately aimed at understanding the influence of: 1) methane lambda, λ_{CH4}, 2) pilot fuel ratio, PR, and 3) charge air temperature on DF combustion.

While the injection and charge air parameters for each of these cases vary and will therefore, be separately tabulated on case by case basis, fuel properties and the general engine operating parameters for both all-metal and optical engines are listed in Table 3. Most of the general engine operating parameters have been established based on past experience at the research facility with these research engines and in line with the demands of this thesis work. It is seen in the table that the diesel pilot injection timing, also referred to as Start Of Injection, SOI in this document, is different for all-metal and optical engine. During early stage parameter verification in all-metal engine, SOI at 8 CAD BTDC produced pilot diesel ignition at 1-3 CAD ATDC. This was considered optimal for combustion studies as the temperature and pressure inside the combustion chamber are maximum at TDC. The same SOI in optical engine however, produced pilot diesel ignition some 6-8 CAD ATDC. The SOI in optical engine was therefore, optimized through tests to bring diesel ignition closer to TDC as in the all-metal engine so that combustion phenomena to be studied optically matched more closely with early stage parameter verification. The optimal SOI for optical engine was hence found to be 15 CAD BTDC.

Table 3. Fuel specifics and engine operation parameters in all-metal and optical engine

Lower heating value, diesel (MJ/kg)	43.4
Lower heating value, methane (MJ/kg)	50
Stoichiometric AFR, diesel	14.5:1
Stoichiometric AFR, methane	17:1
Engine speed (rpm)	1400
Diesel injection pressure (bar)	860
Charge air pressure, gauge (bar)	0.1
Methane overpressure on charge air pressure in manifold (bar)	2.4
Diesel pilot injection timing, SOI (CAD BTDC)	8 in all metal, 15 in optical
Fast measurement in engine (at 0.2 CAD intervals at all engine speeds)	Cylinder pressure, valve positions
Slow measurements in engine (1 Hz)	Flow rates, temperatures, manifold and fluid pressures

In the early stage parameter verification with all-metal engine, various diesel pilot and methane quantities as well as charge air flow rates were tested to check the peak cylinder pressures and cyclic variations. From these tests, it was resolved that when the total injected energy exceeds 150 MJ/h (i.e. equivalent to 3.46 kg/h diesel flow) and λ_{CH4} is close to 2, peak cylinder pressures are above 90 bar. With this information available, the total injected energies

during case studies in the optical engine were kept below 150 MJ/h to prevent failure of glass window from pressure loads. Furthermore, no noticeable performance degradation was observed in injector with 7/9 nozzle holes welded when it was compared against the performance of unmodified 9 hole nozzle injector. The injector with 7/9 nozzle holes welded gave possibility to use diesel flows as low as 0.35 kg/h meaning PR as small as 11.5% could be used in case studies.

It was also found that the charge air feed system (explained in section 3.1.2) and engine gas exchange system (intake port shapes and feasible minimum intake valve lifts put together) available at the research facility allowed intake air mass flows only as low as 44 kg/h at a charge air pressure of 0.1 bar, gauge (lowest feasible pressure). Thus, the minimum air mass flow rate possible for the system, minimum diesel mass flow possible from injector and maximum energy that can be charged into the cylinder without the likelihood of breaking the glass piston window of optical engine altogether define the range of variant parameters that can be used in case studies. As such, λ_{CH4} is set at a range of 1.1 to 1.9, PR at a range of 12.8 to 24.4 and charge air temperature at a range of 28 ºC to 70 ºC.

3.3.2 Parameter setup for case studies

Charge air mass flow and injection (diesel and methane) parameter variants used in three different case studies are detailed using tables in this section.

Case study A: Effect of methane lambda on dual-fuel combustion

The influence of λ_{CH4} on DF combustion was studied by setting up six different cases where λ_{CH4} was varied from 1.1 to 1.9. In order to be within the limits of maximum 'safe' pressure load in the optical engine, it was always attempted to operate with charge air mass flow rates close to the minimum that was feasible in the system. Thus, with less degree of freedom for varying the charge air mass flow rate, in order to vary $\lambda_{CH4,}$ the injection quantity of methane had to be varied. This resulted in different total injected energies in different cases but the targeted methane lambdas were achieved and the analysis of dual-fuel combustion as a function of methane lambda was possible. Similarly, for simplicity and for the fact that diesel injector opening duration corresponding to flow rate of 0.40 kg/h was validated in the early stage parameter verification, the diesel pilot injection quantity was kept constant at that flow rate throughout the different cases. This resulted in PR to lie within a range of 12.2% to 17.6% in these tests. Case specific charge air mass flow and injection parameters for case study *A* are tabulated below in Table 4.

Table 4. Methane lambda, charge air mass flow and injection parameters for case study A

Case name	**Methane lambda, λ_{CH4}**	Diesel pilot		Methane flow		Air mass flow (kg/h)	Total injected energy (kJ/cycle)	Dual-fuel lambda, λ_{DF}
		(kg/h)	(mg/cycle)	(kg/h)	(mg/cycle)			
A1	**1.1**	0.40	9.52	2.50	59.52	46.7	3.39	**0.97**
A2	**1.25**	0.40	9.52	2.35	55.95	49.9	3.21	**1.09**
A3	**1.4**	0.40	9.52	2.23	53.10	53.0	3.07	**1.21**
A4	**1.5**	0.40	9.52	2.08	49.52	53.0	2.89	**1.29**
A5	**1.6**	0.40	9.52	1.97	46.91	53.6	2.75	**1.36**
A6	**1.9**	0.40	9.52	1.62	38.57	49.6	2.34	**1.49**

Case study B: Effect of pilot fuel ratio on dual-fuel combustion

In case study *B,* the influence of PR on DF combustion was studied by using three different cases of PR as stated in Table 5. PR was varied by injecting different quantities of pilot which was possible by using different injection durations (duration of 0.4 ms for B1; 0.55 ms for B2; and 0.65 ms for B3). While in all three cases PR was varied by keeping the total injected energy approximately the same, in two cases B1 and B2, the resulting λ_{CH4} was also kept constant. This sort of parameter setup was employed with a goal to help establish the influence of PR on dual-fuel combustion independent of the effect of rival variant parameters.

Table 5. Pilot fuel ratio, charge air mass flow and injection parameters for case study B

Case name	**Pilot fuel ratio, PR (%)**	Diesel pilot			Methane flow		Air mass flow (kg/h)	Total injected energy (kJ/cycle)	Methane lambda, λ_{CH4}
		(kg/h)	(mg/cycle)	Inj. Duration (ms)	(kg/h)	(mg/cycle)			
B1	**12.8**	0.35	8.33	0.40	2.05	48.81	54.0	2.81	1.55
B2	**20**	0.55	13.1	0.55	1.90	45.24	50.1	2.83	1.55
B3	**24.4**	0.67	15.95	0.65	1.80	42.86	52.0	2.84	1.7

Case study C: Effect of charge air temperature on dual-fuel combustion

The influence of charge air temperature on DF combustion was studied in case study C by varying the temperature of the intake air on four different levels. As can be seen in Table 6, in cases C1-C4, these four charge air temperatures (28, 37, 59 and 70 ^{o}C) were tested against relatively higher λ_{CH4} (1.8) and in cases C5-C8, they were tested against lower λ_{CH4} (1.1). Such a parameter setup was employed because it was seen during early stage parameter verification that at both richer and leaner sides of AFR , there were relatively bigger cycle-to cycle variations in terms of cylinder pressures and also longer ignition delays (estimated roughly by looking at the onset of rapid pressure rise) in DF combustion.

Table 6. Charge air temperature, air mass flow and injection parameters for case study C

Case name	**Charge air temp. (°C)**	Diesel pilot		Methane flow		Air mass flow (kg/h)	Total injected energy (kJ/cycle)	Methane lambda, λ_{CH4}
		(kg/h)	(mg/cycle)	(kg/h)	(mg/cycle)			
C1	**28**	0.40	9.52	1.65	39.29	50.5	2.40	**1.8**
C2	**37**	0.40	9.52	1.61	38.33	49.3	2.34	**1.8**
C3	**59**	0.40	9.52	1.75	41.67	53.6	2.49	**1.8**
C4	**70**	0.40	9.52	1.61	38.33	49.3	2.34	**1.8**
C5	**28**	0.40	9.52	2.68	63.81	50.1	3.60	**1.1**
C6	**37**	0.40	9.52	2.55	60.71	47.7	3.44	**1.1**
C7	**59**	0.40	9.52	2.65	63.10	49.6	3.56	**1.1**
C8	**70**	0.40	9.52	2.51	59.76	46.9	3.40	**1.1**

The three case studies outlined here are expected to demonstrate varying combustion characteristics in terms of the pressure rise rates, shape of HRR curves, onsets of ignition and flame front propagation and thus, provide a solid background for DF combustion characterization.

3.3.3 Test procedures and result processing

In the early stage of this thesis work, all-metal engine was used to test wide range of injection and charge air mass flow parameters that led to their verification. Since the engine could be rotated without any injection, charge air mass flow rates corresponding to different charge air pressures and intake valve lifts were validated by stabilizing them for few minutes and noting down the measured values. In each parameter verification test, diesel injection was then initiated after the charge air mass flow and therefore, the motored pressure at TDC had stabilized. Diesel flow rates corresponding to different injection durations (including the minimum possible for injector) were then noted after stabilizing the flow for few minutes. The measurement of diesel flow rate in this engine at different injector opening durations was important because very small flow rates resulting from the use of skipfire protocol in optical engine was not possible to measure accurately with the available flowmeter and thus, this measurement had to be relied upon in optical engine as well. After stabilizing diesel pilot flow rate at each test-point for about 2 minutes, methane injection was initiated in the engine and the engine now operated in dual-fuel mode. Average methane mass flow rate corresponding to different injector opening durations were also recorded after stabilizing each of them for 2-3 minutes. In each test, cylinder pressures measured at 0.2 CAD intervals were recorded in a file from at least 100 consecutive cycles at stabilization. Cylinder pressure curves were then plotted to primarily check peak pressures and cyclic variations at each tests having their own PR, λ_{CH4} and λ_{DF}.

The optical engine can be run only for short durations. Stabilization of charge air mass flow by rotating the engine before any fuel injection took 1-2 minutes. After the charge air mass flow was stable, diesel pilot injection was initiated. Once diesel pilot injection was initiated, the engine control program took care of ensuring that the injection is made once every seventh cycle and that the camera is also triggered per each diesel pilot injection event. Immediately, after diesel pilot injection, methane injection was also initiated by the user in the engine control program. After 15-25 combustion (injection) cycles, first methane, then diesel injection was

turned off. Thus, in each test-point, dual-fuel cycles in the middle were preceded and succeeded by 1-3 diesel pilot only cycles. This provided for a good comparison between diesel and dual-fuel cycles of the same test-point whenever required. Cylinder pressures at 0.2 CAD intervals and 75-100 images per trigger at 1.4 CAD intervals were automatically recorded by the engine control program in each test-point. The glass window of the piston was cleaned after every 10-12 test-point runs.

Recorded cylinder pressures were saved as columns of data in a text file. Number of columns corresponded to the number of cycles recorded. These data columns were further processed using programs built in Matlab environment for producing cylinder pressure, HRR and cumulative HR curves for either average of dual-fuel and diesel only cycles (separately) of a test-point or for particular cycle when required.

Recorded images from each test-point were also post-processed using programs built in Matlab. Matlab reads each grayscale image as an array of size equal to its resolution and where each element corresponds to a pixel with certain intensity value. The major image processing actions made were noise removal and image enhancement. It was found that the second image of each test point, which is some CADs before the onset of diesel ignition and thus devoid of any NL signal, contained some noisy background. So, the noise removal from images was done by subtracting this image from all other subsequent images. As a result, the remaining information in all images were just the NL signals devoid of any external noise. Image enhancement on the other hand, was simply the process of multiplying the intensity arrays corresponding to images with some multiplier so that NL signals become more pronounced and visible in different forms of displays.

The significance of using programs built in Matlab were that the same routine could be repeatedly applied for post-processing all test points and that the matching of engine data (e.g. cylinder pressure) with image sequences was fully computerized rather than manual and tedious. Additionally, animations containing both cylinder pressure and visuals of combustion process could be produced routinely for demonstration purposes.

The experimental methods used in this thesis work provide basis for analyzing dual-fuel combustion based on cylinder pressure traces, heat release rates, pressure rise rates and accompanying NL images of combustion.

3.4 Terms, calculations and analysis of cylinder pressure data

3.4.1 Dual-fuel combustion related parameters and calculations

Fuel mass flow rate, $\dot{m}_f$ ($\dot{m}_{diesel}$ for diesel and $\dot{m}_{CH4}$ for methane) and air mass flow rate, $\dot{m}_{air}$ are always measured automatically during engine runs amongst numerous other parameters. Thus, when a fuel's lower heating value, LHV is known, both energy flow rate and pilot fuel ratio can be calculated using the fuel mass flows.

The expression for energy flow rate, $\dot{E}$ becomes:

$$\dot{E} = LHV \times \dot{m}_f \tag{3.1}$$

With the energy flow rates for diesel ($\dot{E}_{diesel}$) and methane ($\dot{E}_{CH4}$) known, the pilot fuel ratio, PR can be then calculated using the expression:

$$PR = \frac{\dot{E}_{diesel}}{\dot{E}_{diesel} + \dot{E}_{CH4}} \times 100\% \tag{3.2}$$

Often, an alternative approach to note the different contributions of pilot (diesel) fuel and methane fuel to total fuel energy is to present an expression for the diesel substitution ratio, SR which marks the ratio by which methane fuel energy substitutes the diesel energy in the total energy flow rate. For example, a DF combustion strategy that uses 95% substitution rate would mean that 95% of the total energy that would otherwise be contributed by diesel fuel comes from methane fuel. So an expression for the substitution ratio becomes:

$$SR = \frac{\dot{E}_{CH4}}{\dot{E}_{diesel} + \dot{E}_{CH4}} \times 100\% \tag{3.3}$$

Lambda, λ is defined as a ratio of the real or measured AFR to the stoichiometric AFR for a given fuel and thus, diesel lambda, λ_{diesel} and methane lambda, λ_{CH4} can be expressed as:

$$\lambda_{diesel} = \frac{AFR_{diesel}}{AFR_{diesel,st}} \quad \text{and} \quad \lambda_{CH4} = \frac{AFR_{CH4}}{AFR_{CH4,st}} \tag{3.4}$$

With the always known stoichiometric AFR values for diesel (14.5) and methane (17), a formula for stoichiometric dual-fuel air to fuel ratio, $AFR_{DF,st}$ which takes into account the combination of stoichiometric AFR values of both fuels can be established as:

$$AFR_{DF,st} = AFR_{CH4,st} \times m\%_{CH4} + AFR_{diesel} \times (1 - m\%_{CH4}) \tag{3.5}$$

The dual-fuel lambda, λ_{DF} then is given as:

$$\lambda_{DF} = \frac{AFR_{DF}}{AFR_{DF,st}} \tag{3.6}$$

In the equation, the real or measured dual-fuel air to fuel ratio AFR_{DF} is simply the total air mass flow divided by the total fuel mass (contribution from both fuels) flow. Alternatively, in this document and elsewhere in literature, fuel-to-air ratio is mentioned which is called the equivalence ratio (ϕ) and is simply the reciprocal of λ.

3.4.2 Temperature and pressure at TDC

In ideal models of CI engine processes, the compression stroke is assumed to be an isentropic process [5]. With this assumption, the temperature, T_{TDC} and pressure, p_{TDC} at the end of the

compression stroke when the piston is at TDC can be calculated by using the following equations:

$$T_{TDC} = T_1 \left(\frac{V_1}{V_2}\right)^{\gamma-1} \tag{3.7}$$

$$p_{TDC} = p_1 \left(\frac{V_1}{V_2}\right)^{\gamma} \tag{3.8}$$

Where, T_1 is the intake temperature, p_1 is the intake pressure, V_1 is the volume of the combustion chamber at the start of compression stroke, V_2 is the volume at TDC and γ is the ratio of the specific heats, c_p/c_v.

3.4.3 Heat release and pressure rise rate calculations

Heat release (rate and cumulative) calculations for the purpose of analyzing quantitatively the progress of combustion process can be made by utilizing measured cylinder pressure versus crank angle data. In order to calculate the heat release rate, it is first assumed that the combustion system (combustion chamber in the compression and expansion strokes of the engine) obeys the first law of thermodynamics for an open system which is quasi static [5]. The first law for such a system is given as:

$$\frac{dQ}{d\varphi} - p\frac{dV}{d\varphi} + \sum_i \dot{m}_i h_i = \frac{dU}{d\varphi} \tag{3.9}$$

where $dQ/d\varphi$ is the heat-transfer rate across the system boundary into the system, $p(dV/d\varphi)$ is the rate of work transfer done by the system due to system boundary displacement, $\dot{m}_i$ is the mass flow rate into the system across the system boundary at location i, h_i is the enthalpy of flux i entering or leaving the system, and U is the energy of the material contained inside the system boundary. In real engine, direct application of Equation 3.9 is not possible because of the system not being exactly quasi static, because of the difficulty to accurately predict heat transfer and because of the presence of crevice regions where cylinder charge are at different conditions from the rest of the combustion chamber [5]. Therefore, an expression for the heat release rate that is formulated below only gives the approximation of the real values and as such, is often called the *apparent* heat release rate.

For this formulation, the cylinder contents are treated as a single open system where the mass flows across the system boundary (with the intake and exhaust valves closed during compression and expansion strokes) are the fuel and the crevice flow. With the crevice flow effect omitted, Equation 3.9 becomes:

$$\frac{dQ}{d\varphi} - p\frac{dV}{d\varphi} + \dot{m}_f h_f = \frac{dU}{d\varphi} \tag{3.10}$$

U and h_f are taken to be the sensible internal energy of the cylinder contents and the sensible enthalpy of the injected fuel respectively. The sensible enthalpy of the injected fuel is negligible and thus can be omitted for this formulation which means that $dQ/d\varphi$ in Equation 3.10 becomes the difference of the chemical energy of the fuel (positive quantity) and the heat transfer from the system (negative quantity) [5]. This leads to:

$$\frac{dQ_n}{d\varphi} = \frac{dQ_{gr}}{d\varphi} - \frac{dQ_{ht}}{d\varphi} = p\frac{dV}{d\varphi} + \frac{dU_s}{d\varphi} \tag{3.11}$$

The apparent *net* heat release rate in Equation 3.11 is the difference of the *gross* heat release rate, $dQ_{gr}/d\varphi$ and the heat transfer rate, dQ_{ht} to the walls of the engine and is equal to the sum of the work done on the piston and the rate of change of sensible internal energy of the cylinder contents.

Furthermore, when the cylinder charge is assumed as an ideal gas, Equation 3.11 becomes:

$$\frac{dQ_n}{d\varphi} = p\frac{dV}{d\varphi} + mc_v\frac{dT}{d\varphi} \tag{3.12}$$

For the ideal gas, $pV=mRT$ holds which gives the following relation:

$$\frac{dp}{p} + \frac{dV}{V} = \frac{dT}{T} \tag{3.13}$$

Equation 3.13 is then used to eliminate T from Equation 3.12 which results into an expression in Equation 3.14 that gives the net heat release rate relying just upon the measured pressure data and instantaneous combustion volume. The instantaneous combustion volume can be easily calculated from geometry as trigonometric formula for instantaneous piston position already exists.

$$\frac{dQ_n}{d\varphi} = \left(1 + \frac{c_v}{R}\right) p\frac{dV}{d\varphi} + \frac{c_v}{R} V \frac{dp}{d\varphi} \tag{3.14}$$

or

$$\frac{dQ_n}{d\varphi} = \frac{\gamma}{\gamma-1} p \frac{dV}{dt} + \frac{1}{\gamma-1} V \frac{dp}{d\varphi} \tag{3.15}$$

In Equation 3.15, γ is the ratio of specific heats, c_p/c_v. A γ value of about 1.35 associated with the temperature of air at the end of compression stroke is considered appropriate for heat release rate analysis in diesel engines. Thus, an analysis of apparent net heat release rate is made numerically at small crank angle steps (0.2 CAD) utilizing Equation 3.15.

The cumulative heat release, *QHR* is then the total heat released in the combustion process which can be obtained by summing up the heat release rates from the start to the end of process time and is expressed as:

$$QHR = \sum_{i=m}^{n} \left[\frac{dQ_n}{d\varphi}\right]_i \tag{3.16}$$

In theory, the cumulative heat release is an integral of the gross heat release rate over the complete combustion process and should be equal to the mass of the fuel injected, m_f times the lower heating value, *LHV* of the fuel. In this analysis, it should be equal to within a few percent only as the heat release rate analysis is not exact and *net* heat release rates have been taken into account rather than the *gross.*

The pressure rise rate, *PRR* can be defined as the increase in pressure in relation to the crank angle as:

$$PRR = \frac{dp}{d\varphi} \tag{3.17}$$

4 Results and discussion

In this Chapter, optical results in the form of NL images and correspondingly thermodynamic results in the form of cylinder pressure traces and heat release rate trends are presented and discussed for all case studies. General information obtained from optical results and a representative case of a complete DF combustion progress seen in NL images are presented in Sections 4.1. and 4.1.1 respectively. In Sections 4.1.2 to 4.1.4, results for case studies are discussed in a detailed manner.

4.1 Optical results

As already mentioned in Section 3.3.1, the diesel pilot SOI in all DF case studies in optical engine was set at 15 CAD BTDC. However, during a diesel spray imaging test performed separately at the end of this thesis work, it was found that in real, the liquid fuel jet commenced to come out of the injector tip approximately 4 CAD later than the requested SOI. This fact has been taken into account in the presentation of all forthcoming results in this thesis. The exact timing of liquid fuel jet coming out of the injector hole is important to be established especially to get correct measures of ignition delays.

Furthermore, as a reference to the reader, a diesel only cycle with pilot fuel (injection duration 0.52 ms) injected at 8 CAD BTDC is presented with NL images in Figure 19 below. In the figure, the positions of the diesel fuel sprays as they come out from two holes of the injector can be clearly marked. In the third picture of the sequence, at 2.05 ms after SOI, the fuel sprays are already very far from the injector tip (compared to them in the second picture in the sequence), have completely vaporized and are being combusted producing strong diffusion flames.

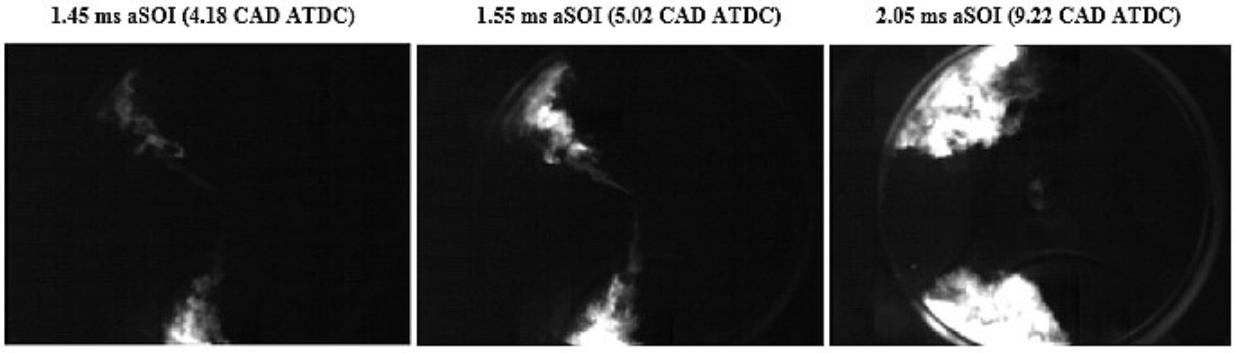

Figure 19. *NL images showing diffusion combustion of sprays in diesel only mode, sprays come out from two open holes of the injector of which seven other holes are clogged by welding*

4.1.1 Flame front propagation in dual-fuel combustion

Figure 20 shows with optical evidence, a generally representative case of a complete DF combustion cycle where the development and subsequent propagation of flame fronts can be clearly seen. All images are from the same combustion cycle in which 75 images were acquired starting from 0.5 ms after SOI signal. The only image processing performed was the multiplication of the NL intensity values by a certain constant multiplier in order to improve the visibility of the images.

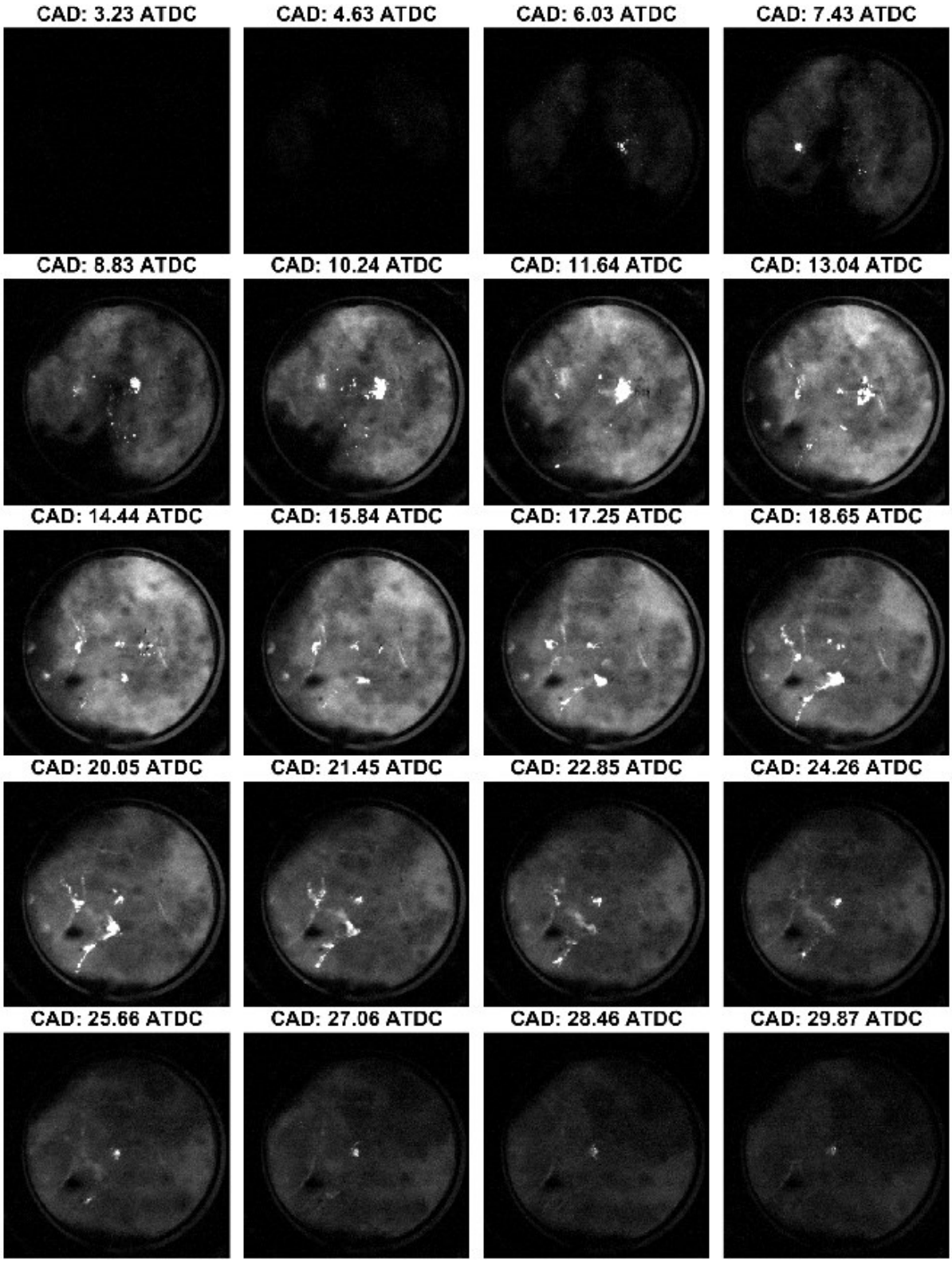

Figure 20. *NL images showing the development and subsequent propagation of flame fronts in DF combustion cycle; pilot injected for 0.42 ms starting from 15 CAD BTDC; CH_4 substitutes for 86.6% of total energy; λ_{CH4} is 1.5 and λ_{DF} is 1.29*

In this DF cycle, pilot fuel was injected for 0.45 ms giving a flow rate of 0.40 kg/h (9.5 mg/cycle) and total methane amount inducted in the cycle was 49.5 mg (at 2.08 kg/h). This resulted in a total injected energy for the cycle to be 2.89 kJ and the pilot fuel ratio, PR to be 14.3%. The air flow rate was set at 53.0 kg/h thus resulting in a λ_{CH4} of 1.5 and λ_{DF} of 1.29.

In the third picture of the sequence corresponding to 6.03 CAD ATDC, two distinct regions of ignition centers separate from each other are visible as first signs of the start of gaseous fuel-air mixture combustion. It is worth noting that these early flames are already close to the walls of the combustion chamber and the central region of the chamber where the injector is located is devoid of any NL. This is probably because the gaseous methane-air mixture gets enough energy for its ignition only by the time the vaporizing diesel sprays have reached the wall where their combustion is seen to be strongest (Figure 19). Furthermore, the centers of two early premixed flame regions at 6.03 CAD ATDC instants are more or less at 10 o' clock and 2 o' clock positions, which are not the original directions of the diesel fuel jets. This is because there is a high level of swirl (swirl number approximately 2.7) resulting from the shape of the intake channels which rotates with high velocity, both the cylinder charge as well as the burning diesel plumes clockwise.

The flames from their early development phase then grow in intensity and propagate towards the center of the combustion chamber where they merge with each other to cover the whole chamber in premixed flame (at 13.04 CAD ATDC). Strong premixed combustion of the methane-air mixture continues until 18.65 CAD ATDC, after which the mixture is almost fully engulfed and the flame slowly commences to terminate. At 29.87 CAD ATDC, the premixed flame has almost completely extinguished. It is worth noting that there is a small and moving intensity saturated area in the center of the combustion chamber that remains radiant even towards the end of the premixed combustion. This results from injector dribbling which creates locally fuel rich zones leading to soot formation, a phenomenon also observed by Dronniou [09], Khosravi [18] and Nithyanandan [30].

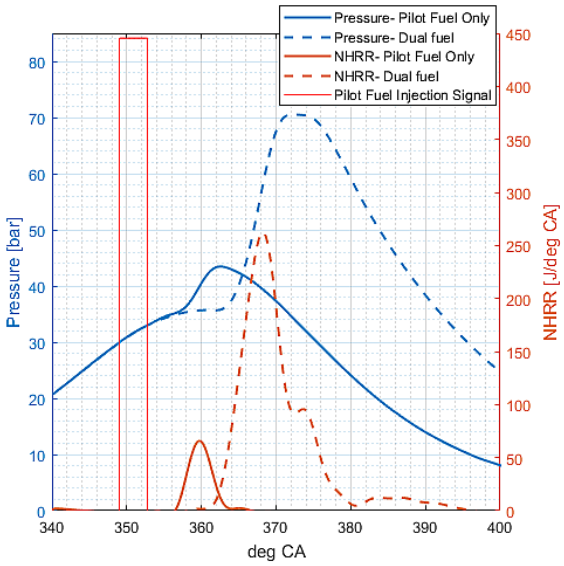

Figure 21. *Cylinder pressure and HRR trend for a DF cycle compared with a diesel only cycle with the same pilot amount. λ_{CH4} is 1.5 and λ_{DF} is 1.29*

Figure 21 shows cylinder pressure and net heat release rate trend for this DF combustion cycle compared with a diesel only cycle from the same test (i.e. same test conditions) and with the

same pilot quantity. The HRR trend clearly shows that in DF cycle, the admission of methane fuel affects the ignition of pilot fuel which provides energy for the onset of combustion of methane-air mixture. There is a considerable prolongation of ignition delay period in DF cycle compared to the ignition delay in pilot fuel only cycle. One approach of defining the ignition delay period in combustion analysis is to define it as a time interval between the SOI and the instant where 5% cumulative heat energy is released. With this approach, the ignition delay in DF cycle in question is 15.6 CAD (1.86 ms) whereas in the pilot fuel only cycle, it is 9.6 CAD (1.14 ms).

This prolongation in the ignition delay period in DF cycle is probably because of the change in preignition reactivity of the diesel pilot brought about by the gaseous fuel which affects the pilot spray kinetics, the intake partial pressure of oxygen and also the physical and transport properties of the mixture [3]. From the viewpoint of chemical kinetics, it has been explained by Masouleh et al. [28] that the addition of methane has an inhibiting effect and reduces the probability of the collisions between diesel and air molecules per unit time delaying the decomposition of diesel and thus leading to an increase in ignition delay period. Observation of the HRR trend of this DF combustion cycle reveals that most of the heat release is contributed by the premixed combustion of methane-air mixture together with some overlapping component from premixed combustion of diesel pilot. This is to mean that the HRR trend is different from the trends seen at high load and longer pilot injection durations for similar engine in Pettinen's work [29] in which the short premixed combustion phase of diesel pilot spray and of methane-air mixture entrained in it is distinguished from the bulk combustion of methane-air mixture that follows. On the contrary, in the DF combustion cycles in this thesis work, the pilot fuel injection durations are relatively short, there are considerably longer periods of ignition delay which means vapors of diesel pilot mix well with surrounding gas-air mixture and consequently their premixed combustion overlap with the premixed combustion of methane-air mixture. This very fact is evidenced by the images in Figure 20 which show absence of any signs of diesel diffusion combustion.

4.1.2 Case study A- Effect of methane lambda

The effect of methane lambda on DF combustion was studied by acquiring crank angle resolved images and corresponding thermodynamic measurements for six different cases of λ_{CH4} as detailed in Table 4. λ_{CH4} is varied from a close to stoichiometric case of 1.1 to leanest case of 1.9. At these ranges of λ_{CH4}, the λ_{DF} ranges from 0.97 to 1.49, respectively. Intake air pressure was kept constant in all cases with an aim to vary λ_{CH4} by keeping the air mass flow constant while only varying the methane mass flow rates. Owing to some variations in engine runs between cases, air mass flows vary by 6.3 kg/h between the smallest flow rate (46.7 kg/h) and the largest (53.0 kg/h) even at the same air pressure. Varying the methane flow rate while keeping the pilot amount same in all cases means that the total injected energies are different in different cases.

Images of DF combustion at five of these six different λ_{CH4} cases are presented in Figure 22. Case A4 where λ_{CH4} equals to 1.5 is omitted for reasons of space in page and because of its similarity with cases A3 and A5 where λ_{CH4} are 1.4 and 1.6, respectively.

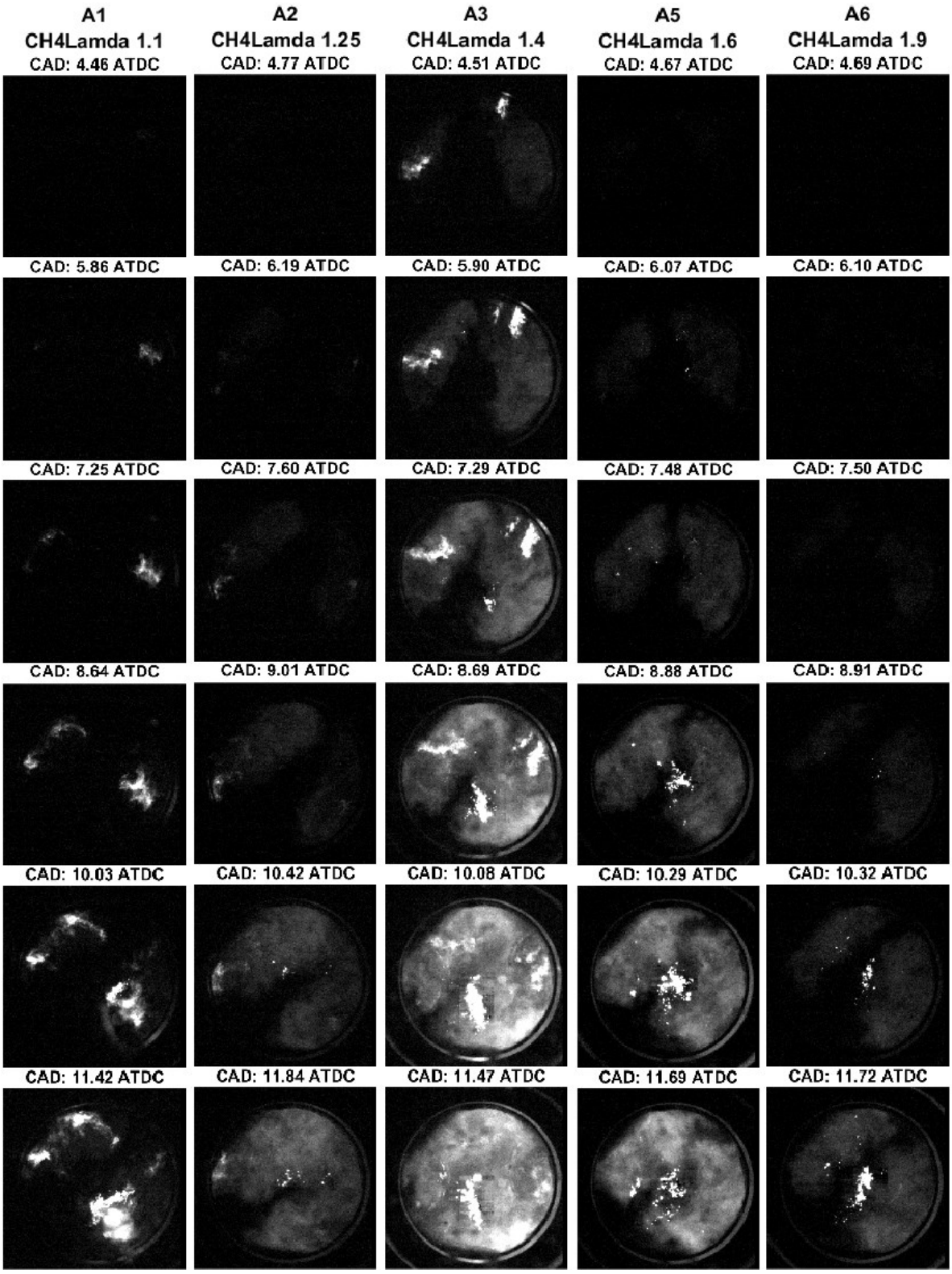

Figure 22. *Images of DF combustion progress for five different cases of λ_{CH4} (Case Study A); images are arranged in columns for each of the λ_{CH4} cases- 1.1, 1.25, 1.4, 1.6 and 1.9.*

For each case in Figure 22, images show the start and development of premixed flame fronts and their subsequent propagation in early phase. A very interesting observation that can be made from the images is that the start of combustion seems to be delayed at the most lean case A6 (λ_{CH4} =1.9) as well as at the least lean case A1 (λ_{CH4} = 1.1) close to methane-air

stoichiometry, compared to that in cases A3, A4 and A5 where λ_{CH4} are 1.4, 1.5 and 1.6, respectively. Relative delays in ignition at cases A1 and A6 are also evident in HRR trends presented in Figure 23. Contrary to the findings in majority of literature (such as [25], [30]) where there is a direct decrease in ignition delay with increasing λ_{CH4}, in this case study, the ignition delay is found to rather show a trend as seen in Figure 24. The first region of descent in the trend (λ_{CH4} = 1.1 to λ_{CH4} = 1.4) showing a decrease in ignition delay with increasing λ_{CH4} is quite the expected phenomenon as availability of more air (or partial pressure of oxygen) promotes the preignition reactivity of diesel pilot leading to an earlier onset of combustion. In other words, at increased methane lambdas where injected methane quantities are relatively smaller, there are less CH_4 molecules to prevent collisions of diesel molecules with air molecules and hence the periods of ignition delays become shorter [28]. The region of ascent in ignition delay trend from case λ_{CH4} = 1.6 to λ_{CH4} = 1.9 however, is rather interesting as it does not seem to follow this theory. An explanation for this countertrend lies possibly in the fact that at higher lambdas (λ_{CH4} >1.6), the overall cylinder temperature becomes lower leading to an increase in ignition delay.

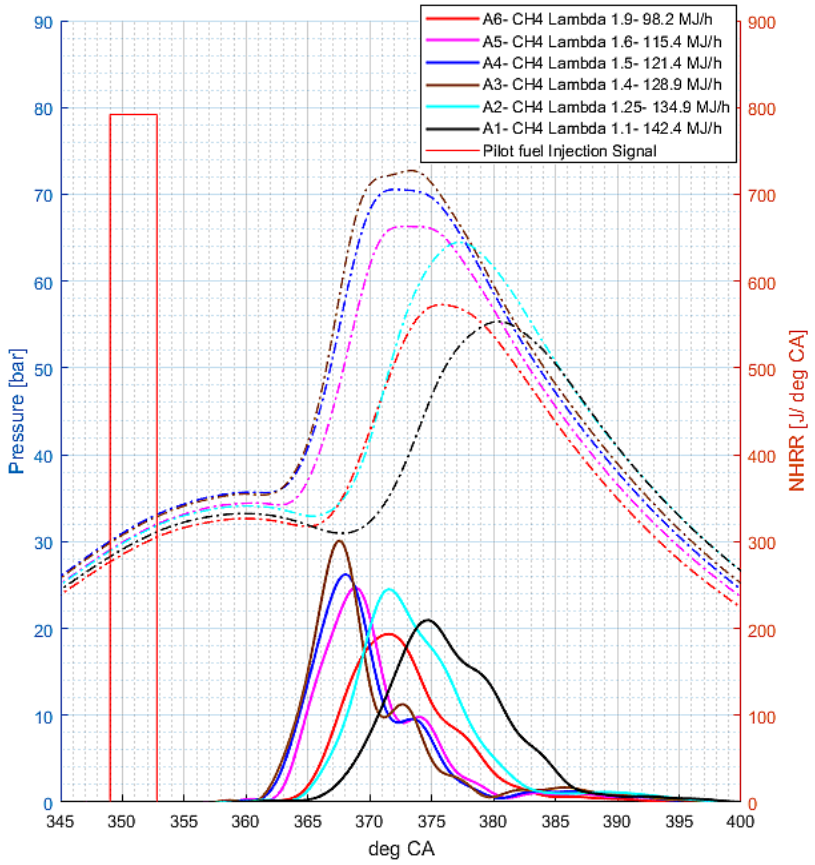

Figure 23. *Cylinder pressure traces and net HRR trends for Case study A- different cases of* λ_{CH4}

HRR trends in Figure 23 as well as the combustion images in Figure 22 show that for cases A3-A5 (λ_{CH4} 1.4 to 1.6), combustion occur faster with steeper rates of energy release in relatively shorter CAD span compared to cases A1 (λ_{CH4} 1.1), A2 (λ_{CH4} 1.25) and A6 (λ_{CH4} 1.9). At case A1 which has the highest amount of methane added of all cases (and thus also the highest total injected energy), the rate of heat release is relatively lower during combustion

which must be due to the decreased reactivity in the diesel pilot spray area, a phenomenon that has also been evidenced by Schlatter et al. [26] through OH* visualizations of n-heptane and methane combustion. At case A6 (λ_{CH4} 1.9), the lower rate of heat release probably signifies the relative difficulty in sustaining flame front propagation at highly lean premixed condition, a fact supported by the weaker NL signals in images even though the optical arrangements were kept the same throughout all the cases. Any misfire, however, was not observed for this case which indicates that the premixed lean limit is not yet reached.

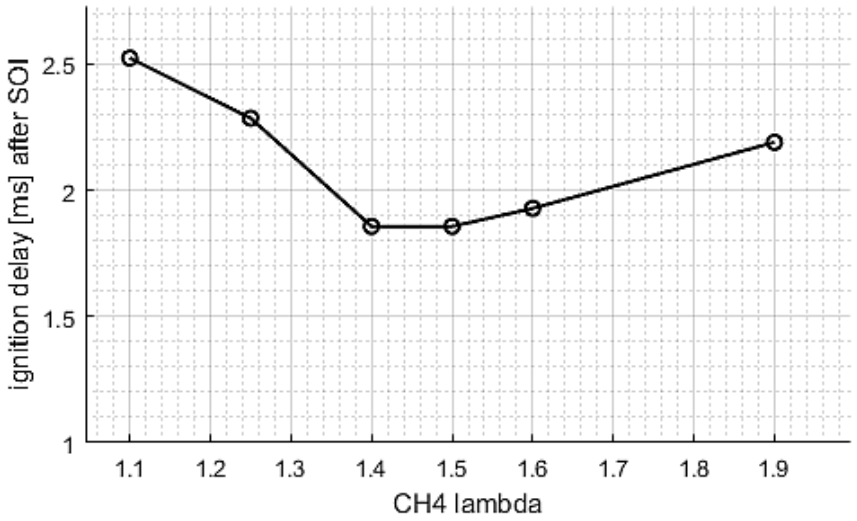

Figure 24. *DF ignition delays for different cases of λ_{CH4}*

Interestingly, cases A3-A5 also seem to show a small second rise in HRR marked between 370 and 375 CADs. This rise could be a sign of *second stage combustion* which is characterized by mass autoignition of the portion of the premixed gaseous fuel-air mixture that has left unburned during the first stage. At the least lean case A1 (λ_{CH4} = 1.1), there's probably less extra oxygen for the oxidation of this portion of mixture and hence a lack of this second rise in HRR. At leanest case A6 (λ_{CH4} = 1.9), there's relatively lower overall temperature during combustion for the unburned portion to autoignite and once again a lack of the second rise in HRR for this case also. Based on the HRR trends seen in Figure 23, it can be concluded that the shape of HRR in DF combustion is strongly dependent upon the λ of premixed fuel. Moreover, at DF conditions such as the ones presented in this section, the profiles of HRR are more similar to those seen in SI combustion behavior [5], suggesting that the premixed combustion is the dominant mode of combustion.

4.1.3 Case study B- Effect of pilot fuel ratio

The effect of pilot fuel ratio (PR) on DF combustion was investigated by varying the pilot fuel amount in the total fuel injected. Three different cases of PR (case B1 at 12.8%, B2 at 20% and B3 at 24.4%) corresponding to different diesel injection durations and therefore, to different diesel amounts were studied. Details of this case study B is given in Table 5 in Section 3.3.2. In the tests, an increase in PR directly corresponds to an increase in the mass of diesel pilot and thus, the balance in total injected energy for all three cases is obtained by decreasing the share of methane fuel as necessary. In cases B1 and B2, by altering the flow rate of air into the cylinder, it was possible to get the same λ_{CH4} for both cases so that the influence of PR on DF combustion can be studied without the rival effect of λ_{CH4}.

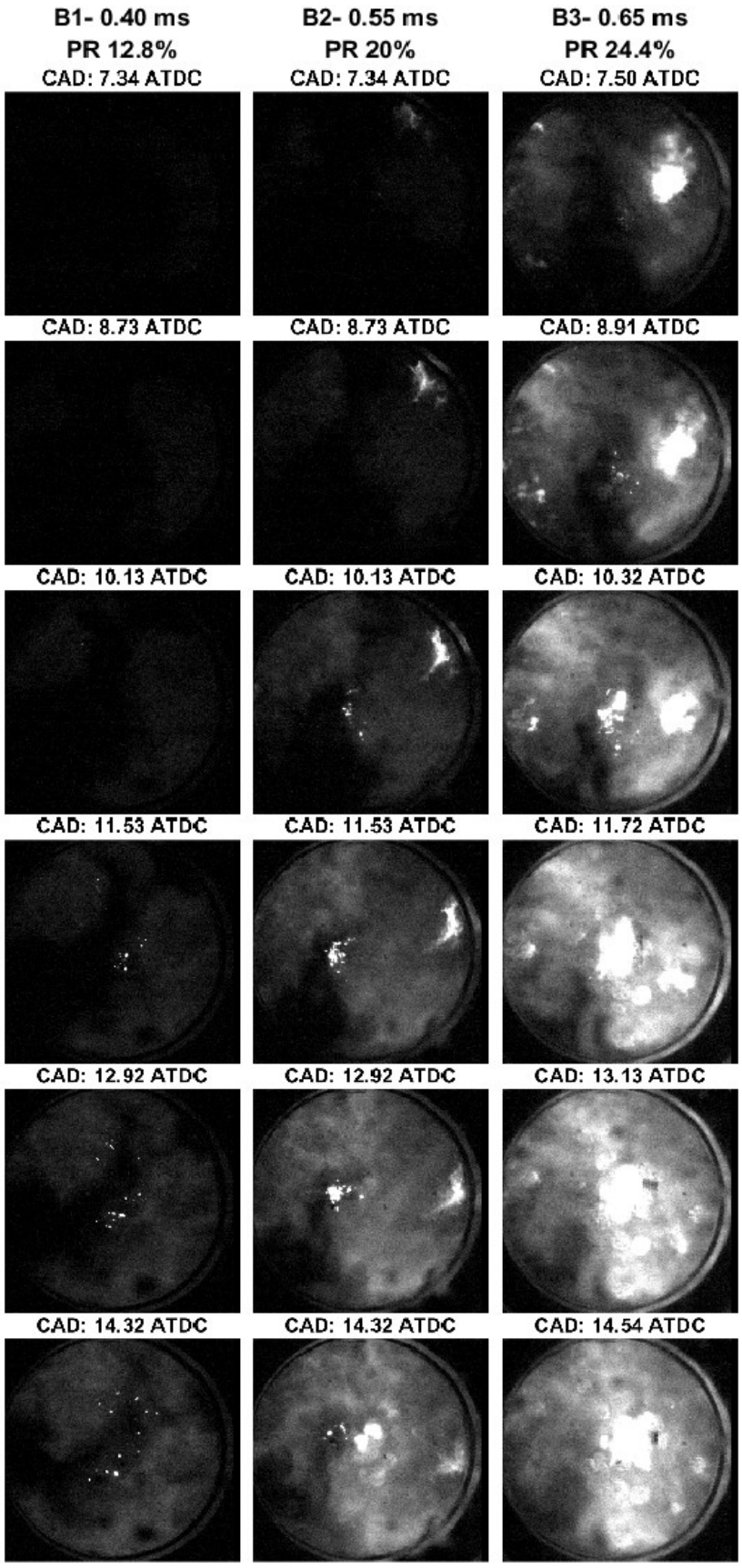

Figure 25. *Images showing DF combustion progress for different cases of pilot fuel ratio (arranged columnwise). Cases B1 and B2 have same λ_{CH4} of 1.55.*

Figure 25 presents crank angle resolved NL images of DF combustion for different cases of PR. The images show the onset of premixed combustion and the growth of two flame fronts until they have covered the whole combustion chamber. As usual, the ignition of premixed methane-air mixture seems to occur in the vicinity of diesel pilot sprays near the cylinder wall. The images show that with increased PR (cases B2 and B3), the NL signals from combustion become more intense, hinting at a presence of probably increased reaction zones in the combustion chamber. Abd Alla et al. [15] have observed that larger pilot amounts provide a greater multitude of ignition centers with larger reaction zones which act as a source of ignition energy for methane-air mixture. Furthermore, with larger pilot amounts, the volume of premixed methane-air mixture entrained in the pilot fuel will also increase and thus, result in an increase in the burn fractions of the premixed mixture and a more successful flame propagation. At higher PR cases B2 and B3, apart from high intensity spots around the injector tip resulting from dribbles, there are localized high intensity burn zones in the regions of vaporized pilot spray hinting at more heterogeneous combustion events. The reason for this could be that when the pilot amounts are large, even with the in-cylinder swirl, the effective mixing of in-cylinder charge is not adequate enough to mix well the pilot fuel, resulting in local fuel rich zones. Moreover, at high PRs, there's probably more likelihood of some diesel pilot fractions to remain unburned even after the start of premixed combustion, which then later burn with high soot radiation. Similar phenomenon has also been observed by Carlucci et al. [31] and Khosravi [18].

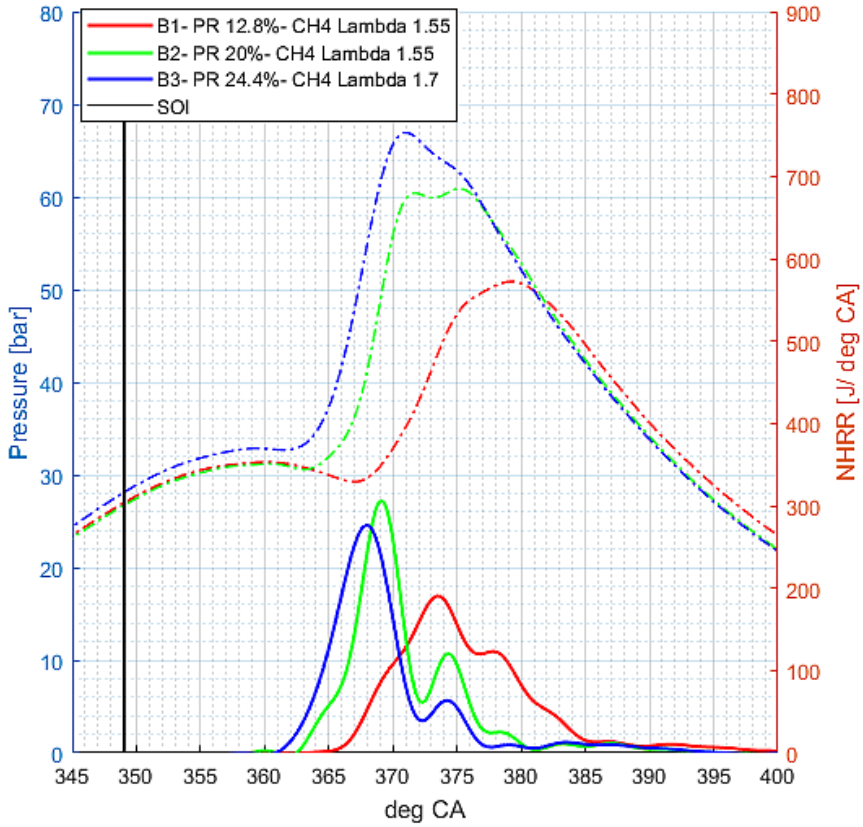

Figure 26. *Cylinder pressure traces and net HRR curves for different cases of PR*

From the HRR curves in Figure 26, it is quite evident that for the injection timing and PR ranges (12.8% to 24.4%) used in this case study, the major peak in HRR in each case study is

a combined contribution from two overlapping combustion modes that seem to occur simultaneously- the premixed combustion phase of diesel pilot and the premixed combustion of methane-air mixture. The second rise in HRR curves for higher PR cases B2 and B3 must once again be a marker of the second stage combustion. It is likely that this second stage combustion is a combination of two events- first, the autoignition of the portion of the premixed fuel that has remained unburned in the first stage which then derives energy from increased pilot amount for autoignition in the second stage, and second, some diffusion burning of the remaining pilot fuel, which in corresponding NL images seem to have burned with soot radiation. With the same total injected energies, the rates of heat release at higher PRs reach higher peaks and span relatively fewer CAD intervals suggesting a more rapid combustion, especially in the early phase.

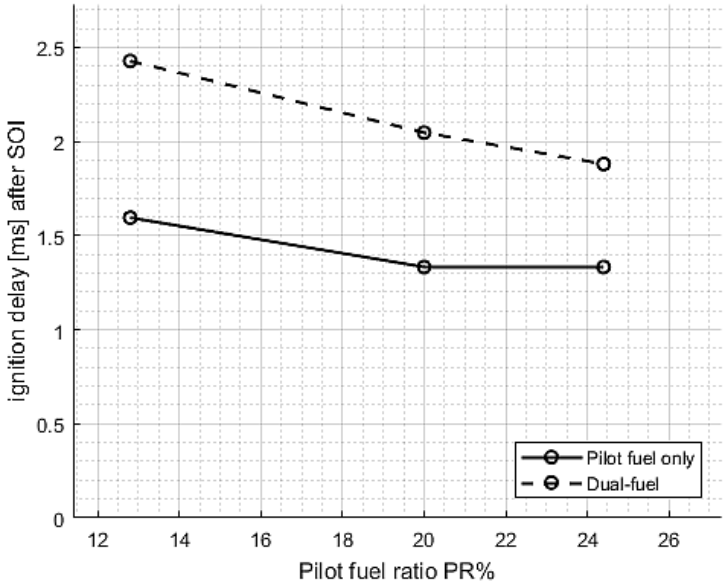

Figure 27. *Ignition delay trends for different PRs*

The HRR curves in Figure 26 also reveal that, to a certain extent, the ignition delay periods in DF combustion decrease with increasing PR or pilot amount. Ignition delays calculated for both DF cycles and pilot fuel only cycles show trends as seen in Figure 27. It is also apparent from the ignition delay trend in Figure 27 that the DF ignition delay is affected more by the gaseous fuel than the diesel pilot amount because, after a certain extent, there's no further decrease in diesel pilot ignition delay with its increasing amount. So, the decrease in ignition delay from B1 (PR 12.8%) to B2 (PR 20%), both of which have the same λ_{CH4}, is certainly facilitated by the increasing PR but the small decrease in DF ignition delay as PR increases from B2 (PR 20%) to B3 (PR 24.4%) which have different $\lambda_{CH4,}$ seems to be rather a result of the decrease in methane amount rather than of the increase in pilot amount.

4.1.4 Case study C- Effect of charge air temperature

The effect of charge air temperature on DF combustion was studied by varying the intake air temperatures at four different levels for each cases of λ_{CH4} 1.8 and λ_{CH4} 1.1. For cases C1 to C4, even though the methane injection duration was set at a constant 9 ms in order to get the same λ_{CH4} that is equal to 1.8, because of some inadvertent variations in engine runs, slightly varying methane flow rates were obtained as seen in Table 6. However, air mass flow rates also varied slightly during engine runs and thus enough number of separate test runs were made to get four cases with the same λ_{CH4} (1.8) and only slightly different total injected energies. Same strategy was applied for cases C5 to C8 where the methane injection duration was 12 ms and resulting λ_{CH4} is 1.1 in all cases. One of the reasons for making a temperature case study at these highly lean and least lean conditions was to investigate the effect of temperature on DF cyclic variations as there were relatively high cycle to cycle variations and even some erratic runs around these methane lambdas compared to, for example, at λ_{CH4} 1.4 or 1.5.

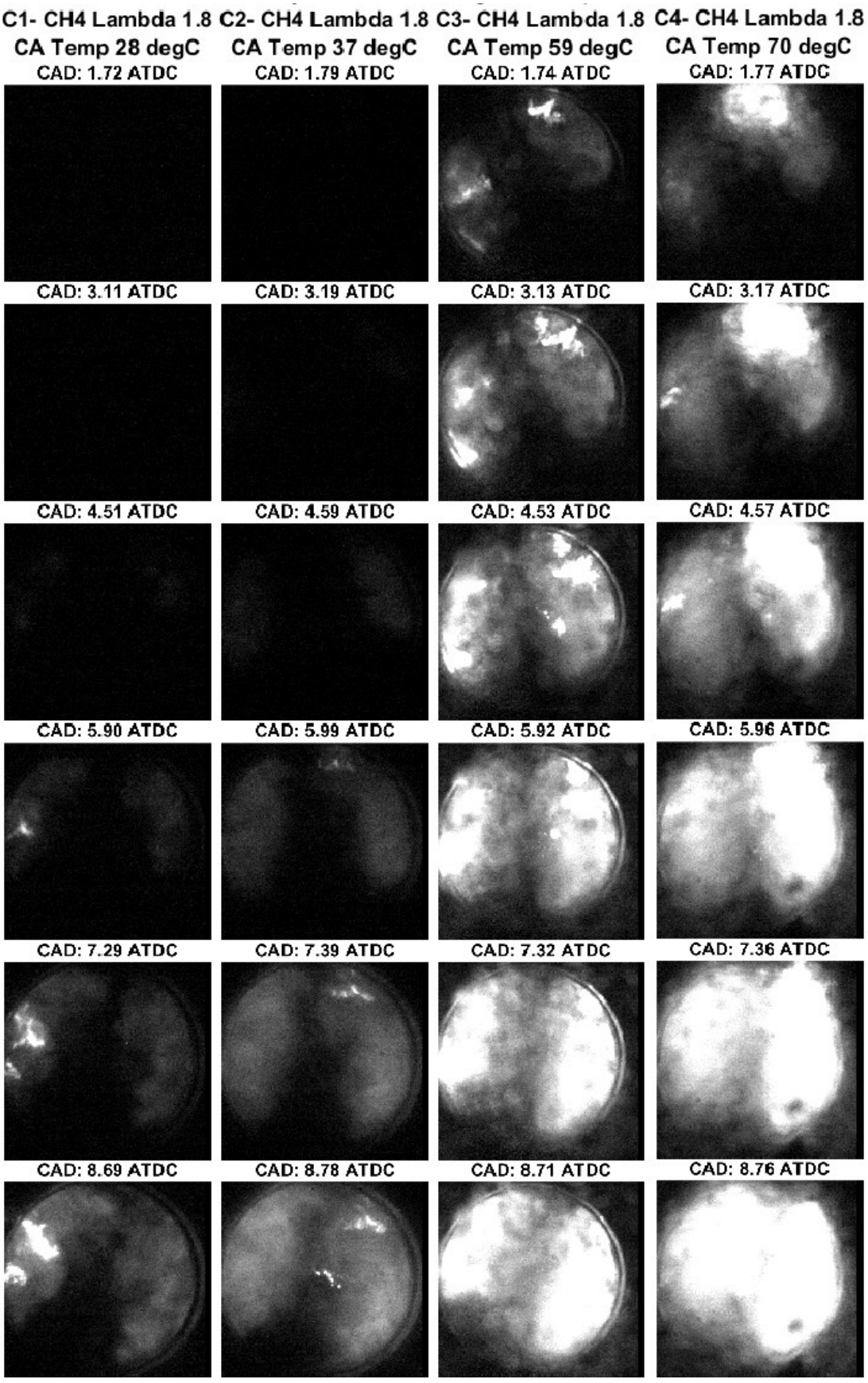

Figure 28. *Images showing DF combustion progress under different charge air temperatures with λ_{CH4} fixed at 1.8. Each column is one case of charge air temperature.*

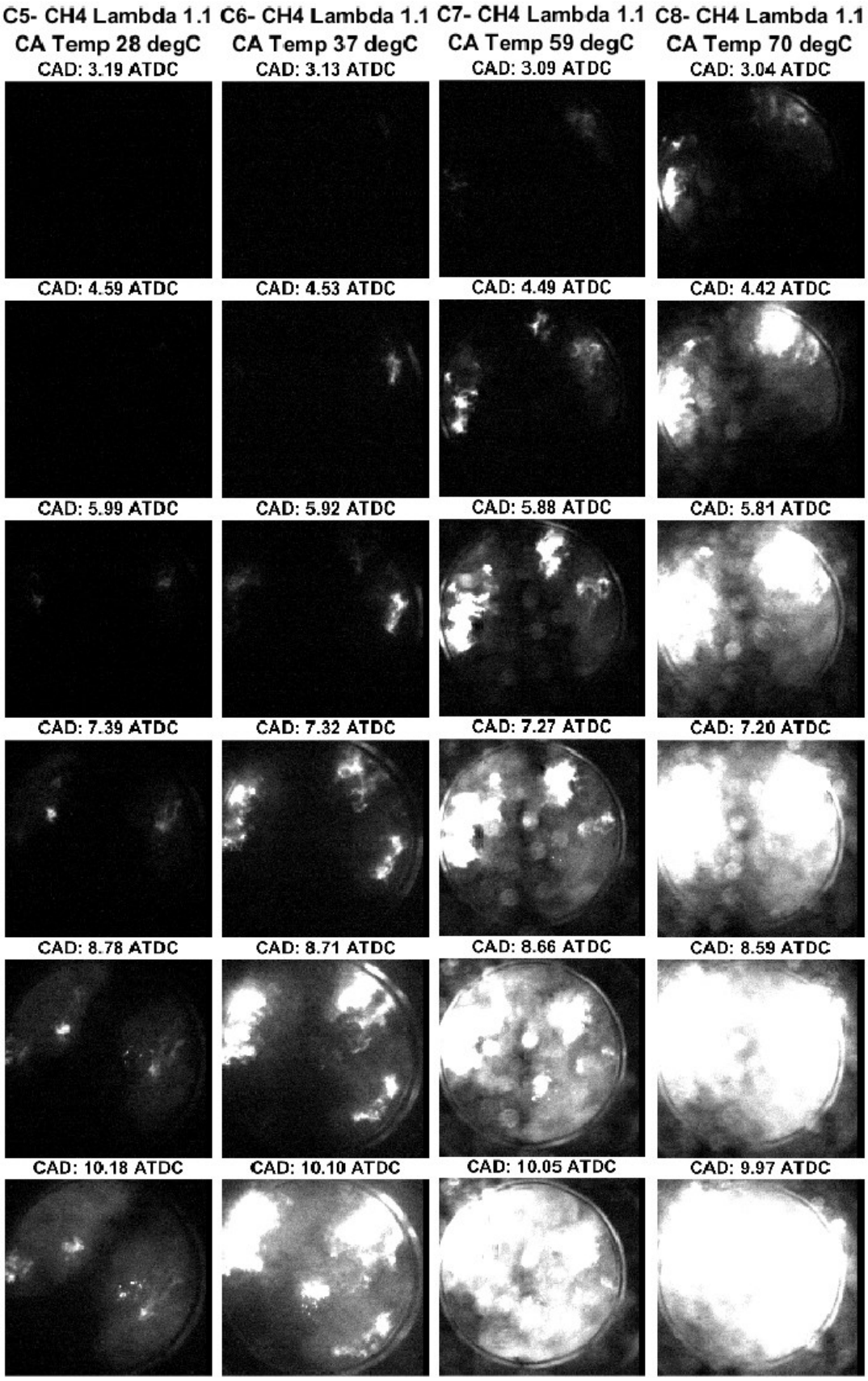

Figure 29. *Images showing DF combustion progress at different charge air temperatures with λ_{CH4} lambda fixed at 1.1. Images are arranged columnwise with different charge air temperatures.*

Figure 28 shows NL images for cases C1 to C4 in all of which λ_{CH4} is 1.8 and intake air temperatures are 28 °C, 37 °C, 59 °C and 70 °C respectively. Similarly, Figure 29 presents NL images for cases C5 to C8 in all of which λ_{CH4} is 1.1 and the intake air temperatures were varied in the same fashion. It is quite evident from both sets of images that increasing the intake air temperature advances the onset of premixed combustion. The trend is further supported by the resulting HRR curves in Figure 30. An increase in intake air temperature translates to a more than linear increase in TDC temperature at the start of combustion. For reference, TDC temperatures for cases C1 to C8, calculated using Equation 3.7 are given in Table 7. Although the geometric compression ratio for the optical engine is 17.9:1, there are some inadvertent leaks from elastic seals, which bring the effective compression ratio down to 14.5. This compression ratio, established by measurement at different intake pressures has been used for calculating the TDC temperatures.

Table 7. Calculated TDC temperatures at different cases of intake air temperatures

Case name	Intake/ charge air temperature		**Calculated TDC temperature**	
	(°C)	(K)	**(°C)**	**(K)**
C1, C5	28	301	**494.4**	**767.4**
C2, C6	37	310	**517.4**	**790.4**
C3, C7	59	332	**573.5**	**846.5**
C4, C8	70	343	**601.5**	**874.5**

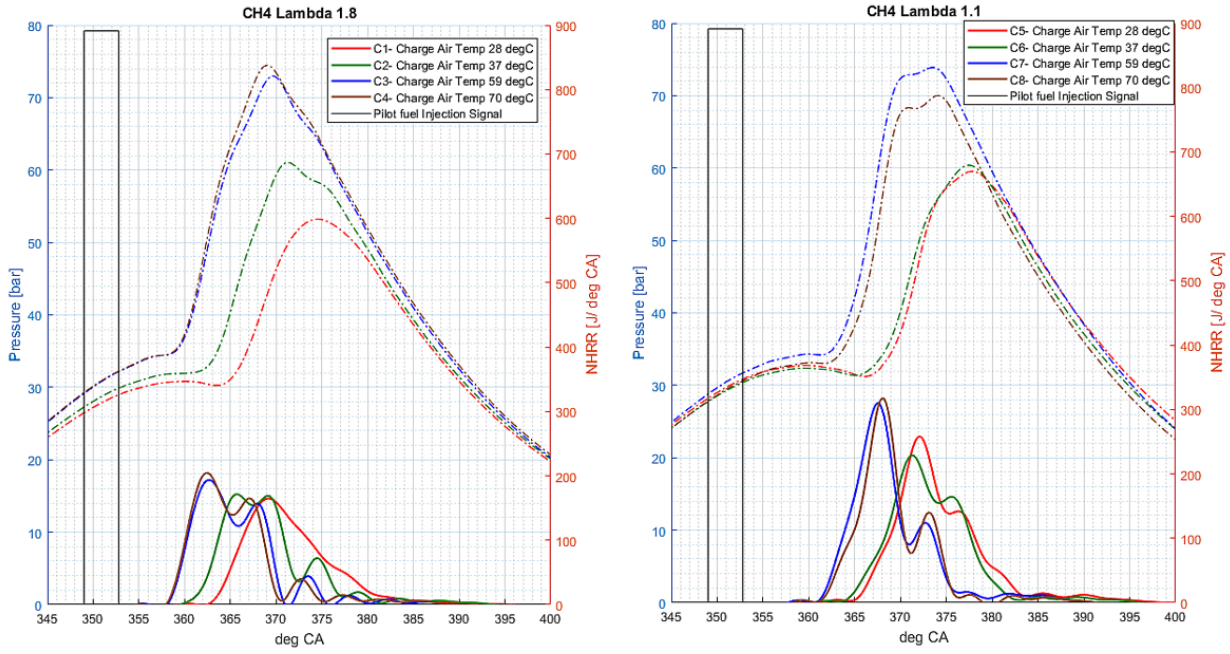

Figure 30. *Cylinder pressure traces and net HRRs for different cases of intake air temperatures- left: at λ_{CH4} 1.8 (cases C1 to C4) and right: at λ_{CH4} 1.1 (cases C5 to C8)*

An increase in TDC temperature is believed to increase the Arrhenius rate of preignition intermediary chemical reactions of diesel pilot and as a consequence, its ignition is brought forward at higher temperatures. This phenomenon is clearly seen in the ignition delay trends in Figure 31, obtained by calculating delays for pilot fuel only cycles corresponding to each

temperature case. As a result of the advance in pilot ignition, the start of premixed combustion also advances at higher temperatures, once again proven by the ignition delay trends of DF cycles seen in Figure 31. While an increase in intake temperature from 28 ºC to 37 ºC and then again to 59 ºC is seen to significantly reduce the ignition delay times for both cases of λ_{CH4}, the later increase in temperature from 59 ºC to 70 ºC does not seem to produce any further significant decrease in diesel pilot ignition delays. Consequently the onset of premixed combustion also does not seem to advance any further at this temperature change region. When the intake air temperature has changed from 59 ºC (332 K) to 70 ºC (343 K), the TDC temperature changes from 846.5 K to 874.5 K. Around these temperatures, the diesel pilot spray is probably showing an NTC (negative temperature coefficient) phenomenon explained by Fu and Aggarwal [32] in their 3-D two phase reacting flow simulation study of diesel sprays. In the NTC region, the diesel spray exhibits a countertrend of rather increasing ignition delay with increasing temperature.

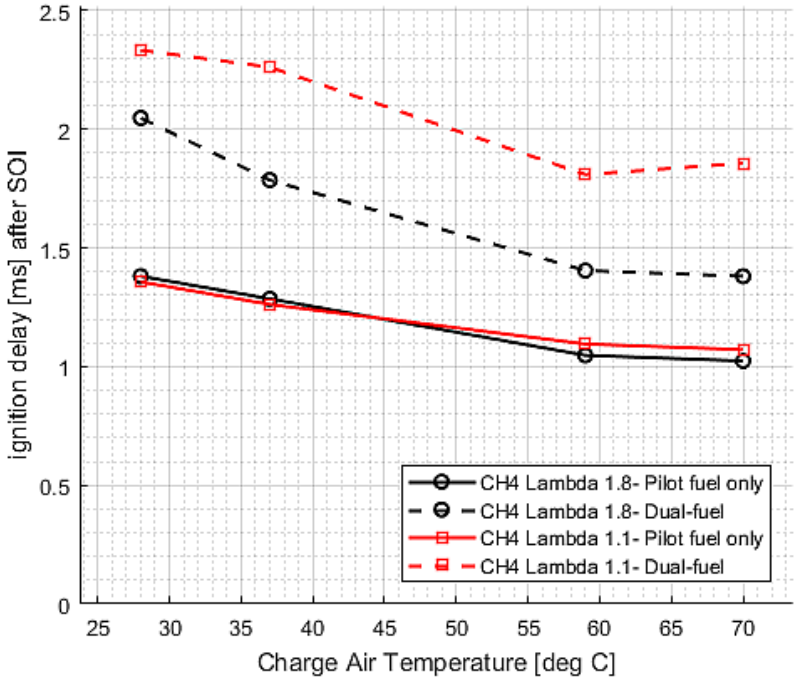

Figure 31. *Ignition delay trends for DF cycles and corresponding pilot fuel only cycles for different intake/ charge air temperatures*

It is seen in Figure 30 that, especially for λ_{CH4} 1.1 condition, as the charge air temperature increases (cases C6, C7, C8), late rises in HRR curves between 370 and 375 CADs become more pronounced. With increased charge air temperature, the in-cylinder temperature also gets higher, providing probably more favorable conditions for autoignition of the remaining premixed fuel- air mixture, or in other words, for second stage combustion. The HRR curves for λ_{CH4} 1.1 also show that at higher temperatures (case C7 and C8), the rate of energy release is higher suggesting a more rapid premixed flame front propagation. At high intake temperatures, the presence of soot radiation zones in NL images (Figure 29) around two spray regions that follow the swirl motion of the charge suggest some occurrence of diesel pilot diffusion combustion.

Interestingly, for λ_{CH4} 1.8 condition at higher intake temperatures (cases C2, C3 and C4), the HRR curves show trends that are different from all other curves seen in the case study results

and which are indeed more similar to the HRR curves of conventional DF combustion. Normally, at highly lean premixed conditions such as at λ_{CH4} 1.8 and at low temperature (case C1), the diesel pilot ignition delay is so long that the well premixed combustion phase of diesel pilot overlaps with the premixed flame front propagation of the methane-air mixture and there is no clear distinction in contribution to HRR from these two overlapping combustion phases. But, when the intake air temperature is increased, the pilot fuel ignition delays are significantly reduced. So, the first peak in HRR contributed by the premixed combustion of diesel pilot and of surrounding gas in its immediate vicinity is distinguished from the second peak in HRR that is contributed by the premixed flame front propagation of methane-air mixture. Perhaps, there's also some contribution to this second peak in HRR from diffusion combustion of diesel pilot as evidenced by soot radiation zones in NL images in Figure 30 between 361 and 368 CADs (1 and 8 CAD ATDC in images) interval. The late rises in HRRs at high temperatures between 370 and 375 CADs must once again be from second stage combustion of the remaining premixed gaseous fuel- air mixture.

Improvements in Cyclic Variations

It was observed during DF combustion tests in this thesis work that at both high gaseous fuel lean conditions ($\lambda_{CH4} > 1.8$) and at conditions close to stoichiometry or richer ($\lambda_{CH4} < 1.1$), there were significant cycle-to-cycle variations which manifest in cylinder pressure traces as presented in Figure 32. It has been mentioned elsewhere in literature, for example in [15] and in [1] that at lean conditions with very low intake temperatures and small pilot injections, there are long ignition delays, weak flame front propagation, possibly some cycles with misfire and as a result erratic engine running. There is however, no mention in literature of huge cyclic variations at close to gaseous fuel stoichiometric conditions as seen in this thesis work. Nevertheless, it is plausible that the higher substitution of energy by methane at these conditions (as λ_{CH4} is brought down by adding more methane while keeping pilot and air flow rate same) has varying effects (e.g. cooling effect) on spray behavior of diesel pilot particularly when its amount is small and thus, brings about variations in ignition delays and peak pressures. As expected, at both highly lean and less lean conditions, increasing the intake air temperature seemed to significantly reduce cycle-to-cycle variations in DF combustion as observed from cylinder pressure traces in Figure 32. However, it should be noted that some degree of cyclic variations in DF combustion is inevitable as the premixed flame growth depends on local mixture motion and composition- quantities which vary in successive cycles in any given cylinder [5].

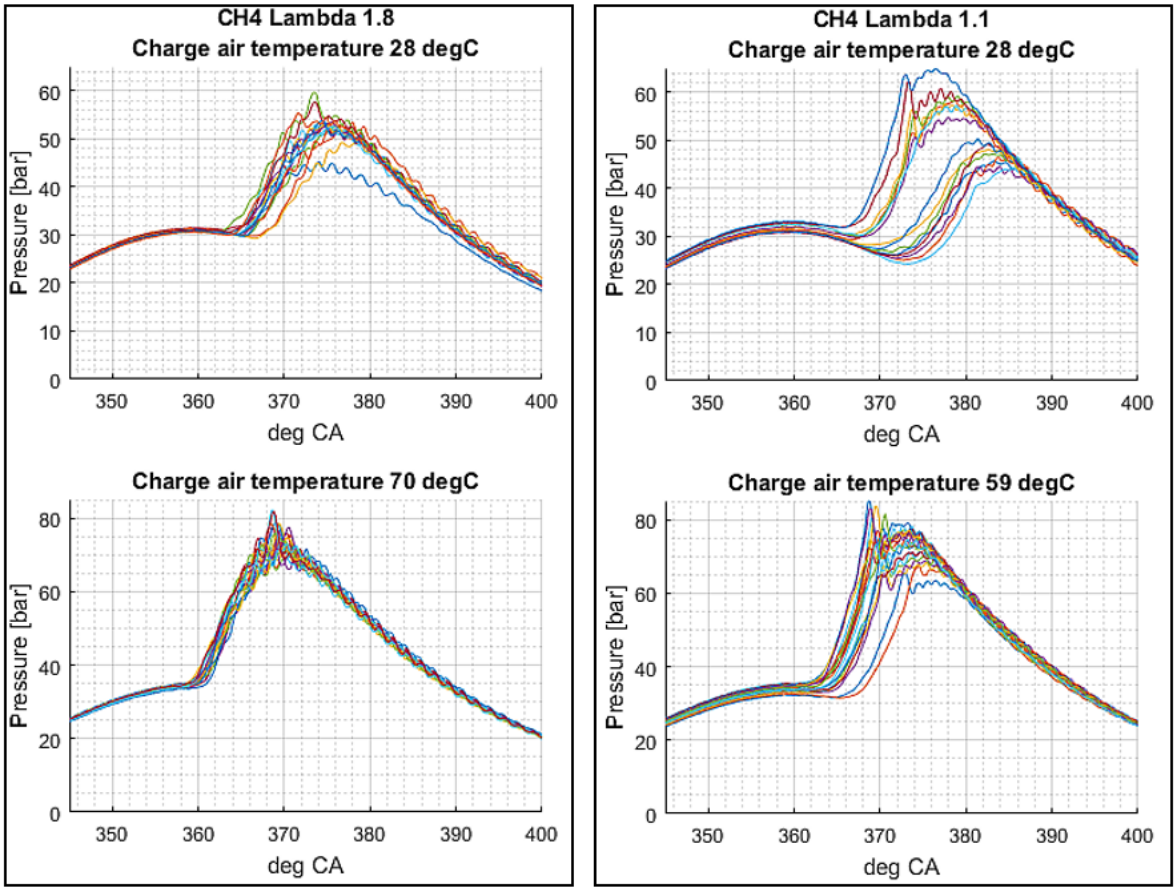

Figure 32. *Cylinder pressures for DF combustion cycles at λ_{CH4} 1.8 and λ_{CH4} 1.1 at different temperatures showing cyclic variations*

PRR at high charge air temperatures

As already discussed in detail in Section 2.3.1, at high loads and when the premixed mixture is too rich, *spark knock* can occur in DF engines. The situation is worsened if the intake air temperatures are higher [1]. During spark knock, cylinder pressures rise at severe rates leading to high temperatures and increased heat transfer that can damage the engine. The DF combustion tests experimented in this thesis work are far from conditions favorable for any spark knock and the resulting pressure traces and NL images also do not reveal any instances of such knock in any of the test cases. However, at high intake temperatures of 59 ºC or 70 ºC used in Case Study C, certain DF cycles show excessive rates of PRR. The cylinder pressure traces and HRR curves presented so far as results in Chapter 4 are averages of the last 4-5 DF cycles in each case study. In doing so, information on certain cyclic abnormalities might get overlooked. Figure 33 presents cylinder pressure traces for certain individual cycles which had DF combustion at high charge air temperatures. Each of these cycles were part of the cluster from which averages were taken.

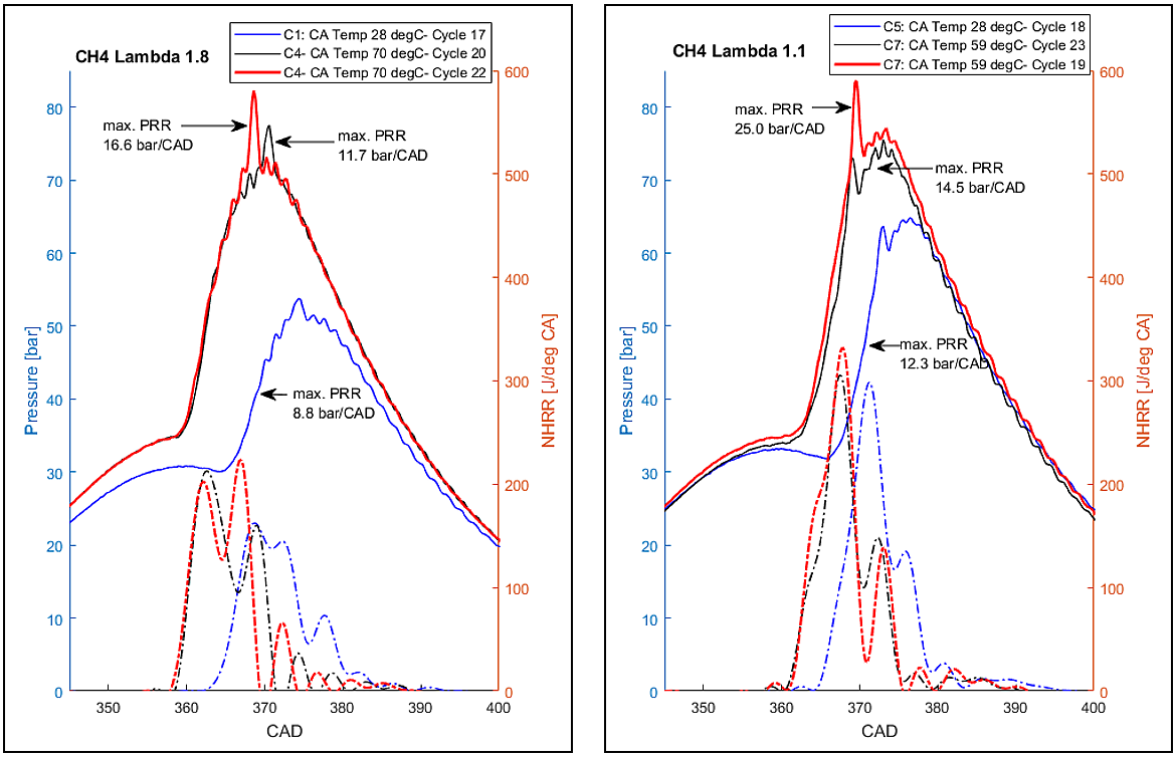

Figure 33. *Evidence of severe PRRs for certain cycles at high intake temperatures- left: at λ_{CH4} 1.8, right: at λ_{CH4} 1.1*

It can be seen in Figure 33 that at high intake air temperatures, certain cycles can have very high PRRs just after the start of (diesel) combustion. The situation is worse for condition that is closer to gaseous fuel stoichiometry. For λ_{CH4} 1.8 case, while the cycle which had intake air temperature at 28 ºC (case C1) shows an acceptable PRR of 8.8 bar/CAD, a cycle from case C4 with intake air temperature 70 ºC shows PRR as high as 16.6 bar/CAD. In common practice, this level of PRR (>10 bar/CAD) is considered excessive in DF combustion [20]. For λ_{CH4} 1.1 case, already at intake air temperature 28 ºC, some cycles show PRR as high as 12.3 bar/CAD. The PRR gets severely excessive when the intake air temperature is raised to 59 ºC, as revealed by one of the cycles from case C7 which has PRR as high as 25 bar/CAD. This phenomenon of excessive PRR in DF combustion just after the start of diesel combustion has been labeled by some as *diesel knock*. In theory, diesel knock occurs when the diesel fuel is injected so early before TDC that the conditions in cylinder have not yet reached sufficient levels to cause its autoignition, and it instead has enough time for forming a premixed mixture. When this premixed mixture eventually burns, pressure rise happens too rapidly, beyond the tolerable limits of engine design. It has already been established through HRR curves and NL images in the preceding sections of this Chapter that the DF combustion tests in this thesis work have shown highly premixed diesel combustion owing to long periods of ignition delays. Hence, it is likely that at high charge air temperatures, in certain cycles, the premixed diesel mixture autoignites with very high PRR that can be recognized as diesel knock.

5 Conclusion

In this thesis work, characterization of DF combustion was done with the help of qualitative and quantitative information obtained from optical and thermodynamic measurements done at varying combustion-related parameters. The crank-angle resolved NL images provide qualitative information about the ignition, premixed flame development and their subsequent propagation. The accompanying thermodynamic measurements and calculations are used to obtain quantitative information such as pressure rise rate, heat release rate and ignition delay. For the engine utilized in this thesis work, fuel amounts used in tests correspond to light load conditions, and this fact has to be thus taken into consideration when drawing conclusions about the DF combustion characteristics. With reference to the main objectives outlined in the beginning of this thesis (Section 1), important observations made in the three case studies of this thesis work are summarized below:

1. NL images show that the premixed flame fronts in DF combustion develop from the evaporated pilot fuel spray regions near the combustion chamber walls and then subsequently propagate towards the center of the combustion chamber.

2. Compared to diesel only combustion mode, the introduction of methane as fuel share significantly lengthens the ignition delay in DF combustion. The extent of increase in ignition delay depends upon the rate of substitution by methane, its concentration in charge and intake air temperature. At various test-points experimented in this thesis, the increase in ignition delay in DF combustion compared to pilot fuel only combustion was in the range of 0.5 ms to 1 ms (Figure 27 and Figure 31). This corresponds to DF ignition delay being 1.5 to 2.0 times longer than the delay in pilot fuel only combustion.

3. With SOI at 15 CAD BTDC in optical tests, the HRR curves in all cases of DF combustion show one major peak that seems to be contributed by two components- the premixed combustion of diesel pilot that overlaps with the premixed flame front propagation. At certain methane lambdas (around λ_{CH4} 1.4 region), higher pilot fuel ratios (PR 20% and 24.4%) and higher intake air temperatures (59 ^{o}C or more), HRR curves show small second rises, considered to be signs of second stage combustion. NL images do not provide adequate information to ascertain what characterizes this second stage combustion.

4. At substitution rates as high as 82% to 88%, when λ_{CH4} was varied from 1.1 to 1.9, DF ignition delay lengthened by 1.5 to 2.0 times compared to pilot fuel only case. Relatively shorter periods of DF ignition delay were observed at λ_{CH4} 1.4 to 1.6 region, with the shortest delay of 1.86 ms observed at λ_{CH4} 1.4 case. NL signals as well as rates of energy release were also relatively higher at these conditions (Figure 22 and Figure 23). At both extremes of the tested methane lambda, the ignition delays were relatively longer- 2.52 ms for λ_{CH4} 1.1 and 2.19 ms for λ_{CH4} 1.9 case. The reason for unexpected increase in ignition delay as the methane-air mixture becomes more leaner from λ_{CH4} 1.4 to λ_{CH4} 1.9 is worth exploring further in future studies.

5. Increased pilot fuel ratio showed only a mild decrease in DF ignition delay. However, with an increase in pilot share in fuel, NL images showed increased number of fuel rich zones and consequent soot radiation.

6. For both λ_{CH4} 1.1 and λ_{CH4} 1.8 cases, higher intake air temperatures (59 ^{o}C and 70 ^{o}C) shortened ignition delays (for e.g. by 1.5 times for λ_{CH4} 1.8 case when temperature was increased from 28 ^{o}C to 70 ^{o}C), promoted second stage combustion and reduced cycle-to-cycle variations. However, higher intake temperatures also resulted in certain DF cycles to have extremely high pressure rise rates- as high as 25.0 bar/CAD in some cycles.

From the available NL evidences and thermodynamic results, it is concluded that at high substitution rates (ca. 85%) and light load conditions as experimented in this thesis, DF combustion is dominated by the premixed flame front propagation rather than by the characteristics of diesel diffusion combustion. It is noted that in future studies, optical investigation of DF combustion could be expanded further so as to get quantitative information in addition to qualitative information about combustion phenomena. Determining ignition delays from heat release rates is less accurate for DF studies which use small amount of pilot such as the ones in this thesis because the filtering of cylinder pressure traces applied in heat release calculations can introduce uncertainties that are in similar magnitude to the heat released by the small amount of pilot. If however, the optical investigation were to be extended so as to obtain chemiluminescence images also, then a more accurate determination of DF ignition delays based on OH* signals would be possible. Furthermore, combining NL images with chemiluminescence and laser based techniques can also give quantitative information such as local equivalence ratios and temperatures based on detection of intermediary species of combustion.

Bibliography

[1] Challen, B. & Baranescu, R., "Diesel Engine Reference Book", 2nd Edition. Butterworth-Heinemann, 1999. ISBN: 0 7680 0403 9

[2] Dronniou, N., Kashdan, J., Lecointe, B., Sauve, K. et al. "Optical Investigation of Dual-fuel CNG/Diesel Combustion Strategies to Reduce CO2 Emissions". SAE Int. J. Engines 7(2):2014. DOI: 10.4271/2014-01-1313.

[3] Karim, G.A. "Combustion in Gas Fueled Compression: Ignition Engines of the Dual Fuel Type". Journal of Engineering for Gas Turbines and Power. ASME, 2003. DOI: 10.1115/1.1581894.

[4] Azimov, U., Tomita, E, and Kawahara, N. "Ignition, Combustion and Exhaust Emission Characteristics of Micro-pilot Ignited Dual-Fuel Engine Operated under PREMIER Combustion Mode". SAE Technical Paper 2011-01-1764. ISSN 0148-7191.

[5] Heywood, J.B., "Internal Combustion Engine Fundamentals", 1st Edition. McGraw-Hill, 1988. New York, NY. ISBN: 0-07-100499-8.

[6] Van Basshuysen, R., Schäfer, F. "Internal Combustion Engine Handbook", 3rd Edition. SAE International, 2002. Wiesbaden, Germany. ISBN: 0-7680-1139-6.

[7] Glassman, I., Yetter, R.A., and Glumac, N.G. "Combustion", 5th Edition. Elsevier, 2015. ISBN: 978-0-12-407913-7.

[8] Dec, J.E. "A Conceptual Model of DI Diesel Combustion Based on Laser-Sheet Imaging". SAE Technical Paper 1997-02-24- 970873.

[9] Flynn, P.F., et al. "Diesel combustion: An Integrated View Combining Laser Diagnostics, Chemical Kinetics, and Empirical Validation'. SAE Congress Paper, 1999. 1999-01-0509.

[10] Sahoo, B. B., Sahoo, N., and Saha, U.K. "Effect of engine parameters and type of gaseous fuel on the performance of dual-fuel gas diesel engines- A critical review". Elsevier, 2008. DOI: 10.1016/j.rser.2008.08.003.

[11] Törmanen, J. "Variable Valve Actuation and Dual-Fuel Combustion". Master's thesis, 2015-08-24. Available from: http://urn.fi/URN:NBN:fi:aalto-201509184411

[12] Pettinen, R. "Dual-fuel combustion characterization on lean conditions and high loads". Master's Thesis ed. Finland: Aalto University, 2016.

[13] Aksu, C., et al. "Extension or PREMIER combustion operation range using split micro pilot fuel injection in a dual fuel natural gas compression ignition engine: A performance-based and visual investigation". Elsevier, 2016. http://dx.doi.org/10.1016/j.fuel.2016.07.120.

[14] Wärtsilä Finland Corporation., "Wärtsilä Medium-Speed Engines"-Brochure. [Online]. [Cited 11.7.2017]. URL: http://pdf.nauticexpo.com/pdf/wartsila-corporation/wartsila-medium-speed-engines/24872-69921.html

[15] Abd Alla, G.H., “Effect of Pilot Fuel Quantity on the Performance of a Dual Fuel Engine”. SAE Technical paper 1999-01-3597.

[16] Karim, G.A., “Dual-Fuel Diesel Engines”, CRC Press, 2015.

[17] Karim, G.A., and Burn, K.S., “The Combustion of Gaseous Fuels in a Dual Fuel Engine of the Compression Ignition Type with Particular Reference to Cold intake Temperature Conditions”. SAE paper 800263, 1980.

[18] Khosravi, M., Rochussen, J., Yeo, J., Kirchen, P. “Effect of Fuelling Control Parameters on Combustion Characteristics of Diesel-Ignited Natural Gas Dual-Fuel Combustion in An Optical Engine”. Proceedings of the ASME 2016 Internal Combustion Engine Fall Technical Conference, ICEF2016-9399.

[19] Kubesh, J. & Brehob, D.D., “Analysis of Knock in a Dual-Fuel Engine”. SAE Technical paper, 1992. Paper Series 922367.

[20] Curran, S.J., Hanson, R.M., & Wagner, R.M., “Reactivity Controlled Compression Ignition Combustion on a Multi-Cylinder Light Duty Diesel Engine.” International Journal of Engine Research, June 01, 2012, vol.13, no. 3. Pp 216-255. ISSN DOI: 10.1177/1468087412442324.

[21] Larsson, A., “Optical Studies in a DI Diesel Engine”. SAE paper 1999-01-3650.

[22] Arnold, A., et al. “DI Diesel Engine Combustion Visualized by Combined Laser Techniques”. Twenty-Fourth Symposium (International) on Combustion/ The Combustion Institute, 1992. pp 1605-1612.

[23] Bladh, H., Brackmann, C., Dahlander, P., Denbratt, I., & Bengtsson, P-E. “Flame Propagation visualization in a spark-ignition engine using laser-induced fluorescence of cool-flame species”. Measurement Science and Technology Journal, 2005. DOI: 10.1088/0957-0233/16/5/006.

[24] Kokjohn, S., Reitz, R., Splitter, D., and Musculus, M., “Investigation of Fuel Reactivity Stratification for Controlling PCI Heat-Release Rates Using High-Speed Chemiluminescence Imaging and Fuel Tracer Fluorescence,” SAE Int. J. Engines 5(2):248-269, 2012, DOI:10.4271/2012-01-0375.

[25] Nithyanandan, K., Gao, Y., Wu, H., Lee, C. et al. “An Optical Investigation of Multiple Diesel Injections in CNG/Diesel Dual-Fuel Combustion in a Light Duty Optical Diesel Engine”. SAE Technical Paper 2017-01-0755. DOI: 10.4271/2017-2017-01-0755.

[26] Schlatter, S., Schneider, B., et al. “N-heptane micro pilot assisted methane combustion in a Rapid Compression Expansion Machine”. Elsevier, 2016. http://dx.doi.org/10.1016/j.fuel.2016.03.006.

[27] Azimov, U., Tomita, E, and Kawahara, N. Diesel Engine- Combustion, Emissions and Condition Monitoring, Saiful Bari ed 2013. “Combustion and Exhaust Emission Characteristics of Diesel Micro-Pilot Ignited Dual-Fuel Engine”. ISBN 978-953-51-1120-7.

[28] Masouleh, M.G., et al. “Comparative study on chemical kinetic schemes for dual-fuel combustion of n-dodecane/ methane blends”. Elsevier, 2017. http://dx.doi.org/10.1016/j.fuel.2016.10.114

[29] Pettinen, R., Kaario, O., and Larmi M., “Dual Fuel Combustion Characterization on Lean Conditions and High Loads”. SAE Technical Paper 2017-01-0759, 2017, DOI: 10.4271/2017-01-0759.

[30] Schlatter, S., Schneider, B., et al. “Experimental Study of Ignition and Combustion Characteristics of a Diesel Pilot Spray in a Lean Premixed Methane/ Air Charge using a Rapid Compression Expansion Machine”. SAE Technical Paper 2012-01-0825. DOI: 10.4271/2012-01-0825.

[31] Carlucci, A.P., “Study of Combustion Development in Methane-Diesel Dual Fuel Engines, Based on the Analysis of In-Cylinder Luminance”. SAE Technical Paper 2010-01-1297. DOI: 10.4271/2010-01-1297.

[32] Fu, Xiao., Aggarwal, S.K., “Two-stage ignition and NTC phenomenon in diesel engines”. Elsevier, 2014. http://dx.doi.org/10.1016/j.fuel.2014.12.059